

Abundances in Stars from the Red Giant Branch Tip to Near the Main Sequence Turn Off in M5. ¹

Solange V. Ramírez ^{2,3} and Judith G. Cohen².

ABSTRACT

We present the iron abundance and abundance ratios for 18 elements with respect to Fe in a sample of stars with a wide range in luminosity from luminous giants to stars near the turnoff in the globular cluster M5. The analyzed spectra, obtained with HIRES at the Keck Observatory, are of high dispersion ($R=\lambda/\Delta\lambda=35,000$). We find that the neutron capture, the iron peak and the α -element abundance ratios show no trend with T_{eff} , and low scatter around the mean between the top of the RGB and near the main sequence turnoff, suggesting that at this metallicity, non-LTE effects are not important over the range of stellar parameters spanned by our sample. To within the precision of the measurements ($\pm \sim 0.1$ dex), gravitationally induced heavy element diffusion does not appear to be present among the stars near the main sequence turnoff studied here. Our work and other recent studies suggest that heavy element diffusion is inhibited in the surface layers of metal poor stars.

Differences in the Na abundance from star to star which extend to the main sequence turnoff are detected in our sample in M5. The anti-correlation between O and Na abundances, observed in other metal poor globular clusters, is not detected in our sample, but it may be hidden among stars with only upper limits for their O abundances. As we found in M71, there is a hint of star-to-star variation in the Zr abundance.

Overall the abundance ratios of M5 appear very similar to those of M71, with the possible exception of the neutron capture element Ba, where we argue that the apparent difference may be due to difficulties in the analysis. As in M71, the α -elements Mg, Ca, Si and Ti are overabundant relative to Fe.

The results of our abundance analysis of 25 stars in M5 provide further evidence of abundance variations among specific light elements at unexpectedly low luminosities, which cannot be explained by our current understanding of stellar evolution.

Subject headings: globular clusters: general — globular clusters: individual (M5) — stars: evolution — stars: abundances

¹Based on observations obtained at the W.M. Keck Observatory, which is operated jointly by the California Institute of Technology, the University of California, and the National Aeronautics and Space Administration.

²Palomar Observatory, Mail Stop 105-24, California Institute of Technology.

³Current Address: SIRTf Science Center, Mail Stop 220-06, California Institute of Technology.

1. INTRODUCTION

Abundance determinations of stars in Galactic globular clusters can provide valuable information about important astrophysical processes such as stellar evolution, stellar structure, Galactic chemical evolution and the formation of the Milky Way. Surface stellar abundances of C, N, O, and often Na, Mg, and Al are found to be variable among red giants within a globular cluster. The physical process responsible for these star-to-star element variations is still uncertain (see the reviews of Kraft 1994 and Pinsonneault 1997, as well as Cohen *et al.* 2001 and Ventura *et al.* 2001).

In order to study the origin of the star-to-star abundance variations, we started a program to determine chemical abundances of the nearer galactic globular cluster stars. In our first series of papers, we studied a sample of stars in M71, the nearest globular cluster reachable from the northern hemisphere (Cohen *et al.* 2001; Ramírez *et al.* 2001; Ramírez & Cohen 2002). Our sample of 25 M71 stars includes stars over a large range in luminosity, in order to study in a consistent manner red giants, horizontal branch stars, and stars at the main sequence turnoff. We measured the iron abundance and the abundance ratios for 23 elements with respect to Fe in our sample of M71 stars, using high dispersion ($R=\lambda/\Delta\lambda=35,000$) optical spectra obtained with HIRES at the Keck Observatory. We found that the $[\text{Fe}/\text{H}]$ abundances⁴ from both Fe I ($[\text{Fe}/\text{H}] = -0.71 \pm 0.08$) and Fe II ($[\text{Fe}/\text{H}] = -0.84 \pm 0.12$) lines agree with each other and with earlier determinations and that the $[\text{Fe}/\text{H}]$ obtained from Fe I and Fe II lines is constant within the rather small uncertainties over the full range in effective temperature (T_{eff}) and luminosity (Ramírez *et al.* 2001). In Ramírez & Cohen (2002), we found that the neutron capture, the iron peak and the α -element abundance ratios show no trend with T_{eff} , and low scatter around the mean between the top of the RGB and near the main sequence turnoff. We detected an anti-correlation between O and Na abundances in our sample of members of M71 which extends to the main sequence. We also observed a statistically significant correlation between Al and Na abundances extending to $M_V = +1.8$, fainter than the luminosity of the RGB bump in M5.

In the present paper, we have studied a sample of 25 stars in the globular cluster M5, again covering a wide range in luminosity. M5 is the nearest intermediate metallicity globular cluster accessible from a northern hemisphere site. We adopt current values from the on-line database of Harris (1996) for its apparent distance modulus at V of 14.31 mag with a reddening of $E(B-V) = 0.03$ mag. Recent CCD photometric studies of this cluster, focusing primarily on its age, are given by Johnson & Bolte (1998) and Stetson *et al.* (1999). Sandquist *et al.* (1996) discuss the predominantly blue horizontal branch of M5. Previous high dispersion abundance studies, the most extensive of which is Ivans *et al.* (2001), include only luminous giant and asymptotic giant branch stars. A study of C and N variations among a large sample of M5 stars at the base of the red giant branch is given in Cohen, Briley & Stetson (2002).

⁴The standard nomenclature is adopted; the abundance of element X is given by $\epsilon(X) = N(X)/N(H)$ on a scale where $N(H) = 10^{12}$ H atoms. Then $[X/H] = \log_{10}[N(X)/N(H)] - \log_{10}[N(X)/N(H)]_{\odot}$, and similarly for $[X/Fe]$.

Important differences with M71 include the lower metallicity of M5, its much lower reddening, its location further from the galactic plane and its larger radial velocity. M5 is more distant than M71, but this is largely compensated by the higher reddening of M71. Hence the apparent brightness at V of stars at a given evolutionary stage is roughly equal in the two clusters.

2. OBSERVATIONS

To the maximum extent possible, the observing strategy, the atomic data and the analysis procedures used here are identical to those developed in our earlier papers on M71 (Cohen *et al.* 2001; Ramírez *et al.* 2001; Ramírez & Cohen 2002).

2.1. The Stellar Sample

Stars were chosen to span the range from the tip of the red giant branch to the main sequence turnoff of M5. This cluster lies considerably further from the galactic plane at $b = -23^\circ$ than does M71, hence field star contamination is a much less serious problem for M5. The photometric database of Stetson *et al.* (1998) and Stetson (2000), which is described in considerable detail in Cohen, Briley & Stetson (2002), was used to verify that the selected stars lie on the cluster locus in various color-magnitude diagrams. For the more luminous stars, we required the assignment of a high probability of membership by Cudworth (1979) in his proper motion survey of this globular cluster. Only reasonably isolated stars were selected.

Throughout this paper, the star names are from Arp (1962) for the brightest stars, from Buonanno *et al.* (1981) or, for the fainter stars previously not catalogued, are assigned based on the object's J2000 coordinates, so that a star with RA, Dec of 15 rm rs.s +2 dm dd is identified in this paper with the name Grmrss_dmdd.

2.2. Data Acquisition and Reduction

All spectra were obtained with HIRES (Vogt *et al.* 1994) at the Keck Observatory. A maximum slit length of 14 arc sec can be used with our instrumental configuration without orders overlapping. Since an image rotator for HIRES is available (built under the leadership of David Tytler), if we can find pairs of program stars with separations less than 8 arcsec, they can be observed together on a single exposure. Pairs were pre-selected to contain two members of the M5 sample. All stars were observed in pairs, except for the very bright star IV-59, for which there was no suitable nearby star with which to form a pair. One set of three suitable stars was found which fit within the maximum allowed slit length.

The desired minimum SNR was 75 over a 4 pixel resolution element for a wavelength near

the center of echelle order 58 ($\sim 6150 \text{ \AA}$). This is calculated strictly from the counts in the object spectrum, and excludes noise from cosmic ray hits, sky subtraction, flattening problems, etc. Since the nights were dark, sky subtraction is not an issue except at the specific wavelengths corresponding to strong night sky emission lines, such as the Na D doublet. This SNR goal was achieved, at considerable cost in observing time, for most of the stars, although we did not meet this goal for the six main sequence turnoff region stars included in our sample. Note that for a fixed SNR in the continuum, for a star of a given luminosity, the lower metallicity of M5 leads to weaker absorption lines, making it difficult to maintain the desired precision of the analysis.

Approximate measurements of the radial velocity were made on line, and if a star was determined to be a non-member, the observations were terminated. Very few non-members turned up in this way. If the probable non-member was the second component in a pair, an attempt was made to switch to another position angle to pick up a different second star, when a possible candidate that was bright enough was available within the limits of the 8 arcsec maximum separation. Through creative use of close pairs, a sample of 27 members of M5 were observed with HIRES, two of which are blue horizontal branch stars in M5; we subsequently ignore them. Figure 1 shows the sample in M5 superposed on a color-magnitude diagram of this globular cluster.

The observations were centered at about 6500 \AA , as were the M71 spectra, with the reddest order reaching the O triplet. Because the HIRES detector is undersized, our spectra do not cover the full length of each echelle order without gaps in the wavelength coverage. We wanted to include key lines of critical elements, specifically the 6300, 6363 [OI] lines, the 7770 O triplet, the Na doublet at 6154, 6160 \AA , and the 6696, 6698 \AA Al I lines. However, it was impossible to create a single instrumental configuration which included all the desired spectral features in the wavelength range 6000 to 8000 \AA , and a single compromise configuration had to be adopted. In particular, although the 6696, 6698 \AA Al I doublet is the most useful feature of that element in this spectral region, we could not get it to fit into a single HIRES setting together with the O lines.

The spectra of the brighter stars in our M5 sample were observed on two nights in June 2000. A 1.15 arcsec slit was used, which provides a spectral resolution of 34,000. All long integrations were broken up into separate exposures, each 1200 sec long, to optimize cosmic ray removal. These data were reduced by Brad Behr using Figaro (Shortridge 1993) scripts with commands written by McCarthy and Tomaney (McCarthy 1988) specifically for echelle data reduction. Observations continued with the same instrumental configuration during three nights in May 2001 to cover the fainter stars in the sample. This set of HIRES data was reduced by JGC using a combination of Figaro scripts and the software package MAKEE⁵.

Table 1 gives details of the HIRES exposures for each star, with the total exposure time for each object. The signal to noise ratio per 4 pixel spectral resolution element in the continuum

⁵MAKEE was developed by T.A. Barlow specifically for reduction of Keck HIRES data. It is freely available on the world wide web at the Keck Observatory home page, <http://www2.keck.hawaii.edu:3636/>.

at 6150 Å is also given, calculated assuming Poisson statistics and ignoring issues of cosmic ray removal, flattening etc. The latter become non-negligible for the very long HIRES integrations necessary to reach as faint as possible in M5. Also listed in the last column is the radial velocity for each star, measured from the HIRES spectra as described in §2.3.

2.3. Radial Velocities

Radial velocities were measured from all the M5 spectra using a list of 36 strong isolated features within the wavelength range of the HIRES spectra with laboratory wavelengths from the NIST Atomic Spectra Database Version 2.0 (NIST Standard Reference Database #78). Using an approximate initial v_r , the list of automatically detected lines, restricted to the strongest detected lines only, generated in the course of measuring the equivalent widths of the lines (see §3) in the spectrum of each of the M5 stars was then searched for each of these features. A v_r for each line was determined from the central wavelength of the best-fit Gaussian, and the average of these defined the v_r for the star. Heliocentric corrections appropriate for each exposure were then applied to the measured v_r ⁶. The radial velocities for our sample of stars is listed in column 6 of Table 1. Based on their measured radial velocities, all the stars of our sample are members of M5. They have a mean v_r of +55.0 km s⁻¹, with $\sigma = 4.3$ km s⁻¹. This is in good agreement with the value of Harris (1996) of $v_r = +52.6$ km s⁻¹. The velocity dispersion we find for M5 is also in good agreement with the published value of 4.9 km s⁻¹ for a large sample of luminous giants from Rastorguev & Samus (1991).

3. EQUIVALENT WIDTHS

The search for absorption features present in our HIRES data and the measurement of their equivalent width (W_λ) was done automatically with a FORTRAN code, EWDET, developed for our globular cluster project. Details of this code and its features are described in Ramírez *et al.* (2001). Because M5 is considerably more metal poor than M71, the determination of the continuum level was easier, and the equivalent widths measured automatically should be more reliable.

A list of unblended atomic lines with atomic parameters was created by inspection of the spectra of M5 stars, as well as the online Solar spectrum taken with the FTS at the National Solar Observatory of Wallace, Hinkle & Livingston (1998) and the set of Solar line identifications of Moore *et al.* (1966). The list of lines identified and measured by EWDET is then correlated, taking the radial velocity into account, to the list of suitable unblended lines to specifically identify the various atomic lines.

⁶While the MAKEE reduction package removes this term automatically, heliocentric corrections must be calculated and explicitly removed from echelle spectra analyzed using Figaro scripts.

In Ramírez *et al.* (2001), we derived $\lambda D - W_\lambda$ relation (where D is the central depth of the line) for the Fe I lines of “the weak line set” (Fe I lines within 2σ of the $\lambda D - W_\lambda$ fit, with $W_\lambda < 60 \text{ m}\text{\AA}$, and errors less than a third of the W_λ) for our analysis of similar spectra in the globular cluster M71. We used these $\lambda D - W_\lambda$ relations to determine “the good line set” (lines with errors less than a third of the W_λ and with W_λ computed from the derived $\lambda D - W_\lambda$ relations) in the M71 data. We have used the same approach for the analysis of the atomic spectral lines present in the spectra of our M5 sample. We computed the $\lambda D - W_\lambda$ fit for each star’s Fe I lines, except for the six faintest stars, where not enough Fe I lines were detected to do so. For the six faintest stars we used for the remainder of the analysis the equivalent widths measured automatically by EWDET. We used the $\lambda D - W_\lambda$ relations to determine “the weak line set” for the Fe I lines and the “the good line set” for the lines of all the elements, except for the O I and Ca I lines, and for the elements that show hyperfine structure splitting (Sc II, V I, Mn I, Co I, Cu I, and Ba II). The equivalent widths of the O I lines were measured by hand, since thermal motions become important at its low atomic weight and the $\lambda D - W_\lambda$ relations derived for Fe I lines may no longer be valid. For Ca I lines and the lines of elements that show hyperfine structure splitting, we used the equivalent widths measured automatically by EWDET, but did not force them to fit the Fe I $\lambda D - W_\lambda$ relationship due to the probable different broadening mechanisms. A few of the Ca I lines were strong enough to be on the damping part of the curve of growth, but only in the spectra of the coolest M5 giants. The W_λ used in the abundance analysis are listed in Table ?? (available electronically).

4. ATOMIC PARAMETERS

The provenance of the gf values and damping constants we adopt in our analysis of M5 stars is discussed below. In general, the atomic data and the analysis procedures used here are identical to those developed in our earlier papers on M71 (Cohen *et al.* 2001; Ramírez *et al.* 2001; Ramírez & Cohen 2002). At the request of the referee, however, we have updated the Solar equivalent widths we use to derive the adopted Solar abundances (see §4.3). Only small changes in the resulting abundances are introduced by these modifications.

4.1. Transition Probabilities

Transition probabilities for the Fe I lines were obtained from several laboratory experiments, including studies of Fe I absorption lines produced by iron vapor in a carbon tube furnace (Blackwell *et al.* 1979, 1982a,b, 1986) (Oxford Group), measurement of radiative lifetimes of Fe I transitions by laser induced fluorescence (O’Brian *et al.* 1991; Bard *et al.* 1991; Bard & Kock 1994), Fe I emission line spectroscopy from a low current arc (May *et al.* 1974), and emission lines of Fe I from a shock tube (Wolnik *et al.* 1971). We also considered solar gf values from Thévenin (1989, 1990) when needed. The Fe I gf values obtained by the different experiments were placed into a common scale with respect to the results from O’Brian *et al.* (1991) (see Ramírez *et al.* (2001) for details). The

gf values for our Fe II lines were taken from the solar analysis of Blackwell *et al.* (1980), Biémont *et al.* (1991a), and from the semiempirical calculations of Kurucz (1993b). For Fe I and Fe II gf values, we used the same priority order for the gf values from different experiments as in Ramírez *et al.* (2001).

Transition probabilities for the lines of atomic species other than iron were obtained from the NIST Atomic Spectra Database (NIST Standard Reference Database #78, see (Weise *et al.* 1969; Martin *et al.* 1988; Fuhr *et al.* 1988; Weise *et al.* 1996)) when possible. Nearly 80% of the lines selected as suitable from the HIRES spectra have transition probabilities from the NIST database. For the remaining lines the gf values come from the inverted solar analysis of Thévenin (1989, 1990), with the exception of La II and Eu II lines (see §4.3). The solar gf values of Mg I, Ca I, Ti I, Cr I, and Ni I were corrected by the factors derived earlier (see Table 3 of Ramírez & Cohen 2002) which are needed to place both sets of transition probabilities onto the same scale. The correction factors were computed as the mean difference in $\log(gf)$ between the NIST and solar values for the lines in common.

Six elements show hyperfine structure splitting (Sc II, V I, Mn I, Co I, Cu I, and Ba II). The corresponding hyperfine structure constants were taken from Prochaska *et al.* (2000).

4.2. Damping Constants

As in our M71 work, the damping constants for all Fe I and Fe II lines were set to twice that of the Unsöld approximation for van der Waals broadening following Holweger *et al.* (1991). Some of the Na I and Ca I lines are strong enough for damping effects to be important. For Na I the interaction constants, C_6 , of the van der Waals broadening were taken from the solar analysis of Baumüller *et al.* (1998). Smith & Raggett (1981) studied collisional broadening of 17 Ca I lines. Comparing their experimental results and the predicted values of C_6 obtained using the Unsöld approximation, we found that the experimental C_6 are comparable to the Unsöld C_6 . Thus for the Ca I we used the experimental C_6 from Smith & Raggett (1981) when available; if not, we set C_6 to be that of the Unsöld approximation. The empirical values of C_6 for Mg I from Zhao *et al.* (1998) are also used. For the lines of all other ions we set C_6 to be twice the Unsöld approximation following Holweger *et al.* (1991).

4.3. Solar Abundances

We need to establish the solar abundances corresponding to our adopted set of gf values and damping constants. We measured our own set of Solar equivalent widths from the online Solar spectrum taken with the FTS at the National Solar Observatory of Wallace, Hinkle & Livingston (1998) using our code EWDET. Solar abundance ratios were then computed using our compilation of atomic parameters, the Kurucz model atmosphere for the Sun (Kurucz 1993a) and this list of

Solar equivalent widths. We adopt $\xi = 1.0 \text{ km s}^{-1}$ for the Sun.

The results are listed in Table 3. The entries in this table are slightly different than the entries in Table 4 of Ramírez & Cohen (2002), calculated for the M71 analysis, since the Solar equivalent widths used in the M71 study were taken from the compilation of Moore *et al.* (1966). Assuming our atomic parameters, Solar model, Solar W_λ and analysis are correct, this calculation should reproduce the current compilation of photospheric solar abundances of Grevesse & Sauval (1998). The difference Δ between our solar abundances and the photospheric solar abundances from Grevesse & Sauval (1998) is listed in column 5 of Table 3. We ascribe small differences to problems in the absolute scale of the adopted gf values. In general, these differences are reasonably small, with the exception of [O/Fe], [Ca/Fe] and [Zr/Fe]. For these three species, we fail to reproduce the Solar abundance by more than 0.1 dex. The difference we found for [Ca/Fe] ($\Delta = -0.16$ dex) is almost the same as the correction factor that needs to be applied to the inverted solar gf values from Thévenin (1989, 1990), none of which were actually used here since all the detected Ca I lines for our M5 sample are included in the NIST database. The NIST gf scale is within 0.08 dex of that of Smith & Raggett (1981), but Smith (1981) claims to reproduce the Solar Ca abundance with their gf values. He achieves this because his Solar W_λ are considerably larger than those of Moore *et al.* (1966) or those measured here. If there is an error in the NIST Ca I absolute gf value scale, then our procedure of comparing to our own Solar abundance will remove it exactly when [Ca/Fe] is calculated for the program stars. However, if the problem lies in how best to measure the W_λ of very strong Ca I Solar lines, our procedure can only remove the error approximately. Furthermore the Solar Ca lines are quite strong, and hence the inferred Ca abundance is somewhat dependent on the choice of damping constant, but that is not the case in general in M5. The O abundance listed in Table 3 corresponds to the solar value derived from the forbidden lines, which are very weak in the Sun. The three Zr I lines, which give $\Delta = +0.29$ dex, are also very weak, but our gf values and Solar W_λ agree reasonably well with those of Biémont *et al.* (1981), who carefully analyzed the Solar Zr abundance. It may be that this is a problem in the details of the temperature gradient in the outermost layers of our adopted model atmosphere (see comments in Biémont *et al.* 1981). If such an error is independent of T_{eff} , this is basically the same as having an error in the scale of the transition probabilities, which would lead to an incorrect Solar $\epsilon(\text{Zr})$, but would not affect any of our results which are expressed at [Zr/Fe].

La II and Eu II are special cases. The Solar W_λ for the single line of Eu II and for those few lines of La II that are detected here or in our M71 sample are extremely weak. There are no gf values in NIST for these lines. We were forced to use the transition probabilities from Corliss & Bozman (1962), adjusted as recommended by Arneson *et al.* (1977), for the three La II lines. Since the submission of our M71 paper, a new analysis of the spectrum of La II has appeared. Lawler, Bonvallet & Sneden (2001) provide transition probabilities, hyperfine structure, and a new determination of the Solar La abundance, but only include one of the three lines used either here or in our analysis of M71 stars. We therefore adopt the Solar La abundance from Lawler, Bonvallet & Sneden (2001), and scale our gf values by +0.10 dex so that they agree with the new one for the

single line in common, at 6390Å. This is the strongest of the three lines, and the only one seen in most of our stars in which La II is detected. For similar reasons, we adopt the gf value of Lawler *et al.* (2001) for the single observed line of Eu II as well as their Solar Eu abundance of Eu.

We use the solar abundances listed in Table 3, derived from our choice of atomic line parameters, to compute the iron abundance and abundance ratios for our sample of M5 stars.

5. STELLAR PARAMETERS

We follow the philosophy developed for M71 and described in Cohen *et al.* (2001). We adopt current values from the on-line database of Harris (1996) for the apparent distance modulus of M5 at V of 14.31 mag with a reddening of $E(B-V) = 0.03$ mag. The relative extinction in various passbands is taken from Cohen *et al.* (1981) (see also Schlegel, Finkbeiner & Davis 1998). Based on the high dispersion analysis of Ivans *et al.* (2001) for a large sample of luminous red giants in M5, we adopt as an initial guess a metallicity for the cluster of $[Fe/H] = -1.0$ dex.

We utilize here the grid of predicted broad band colors and bolometric corrections of Houdashelt, Bell & Sweigart (2000) based on the MARCS stellar atmosphere code of Gustafsson *et al.* (1975). In Cohen *et al.* (2001) we demonstrated that the Kurucz and MARCS predicted colors are essentially identical, at least for the specific colors used here.

The observed broad band V and I colors for each program star from the photometric database of Stetson *et al.* (1998) and Stetson (2000), corrected for extinction, are used to determine T_{eff} . The set of models with metallicity of -1.0 dex, nearest to our initial estimate of $[Fe/H]$, is used. Table 4 lists the T_{eff} thus deduced. The reddening to M5 is small, making possible extinction variations across the cluster irrelevant. We assume an random photometric error of 0.02 mag applies to $V - I$ from Stetson (2000). Following Cohen *et al.* (2001), this translates into a total uncertainty in T_{eff} of 75 K for giants rising to 150 K for main sequence stars using $V - I$. One can obtain a reasonable guess as to the magnitude of possible systematic errors in Peter Stetson’s photometric database for M5 by comparing the first and second versions of his catalog; there appear to be mean differences in the photometric zero points of ~ 0.02 mag, corresponding to a mean difference in T_{eff} of ~ 75 K.

We have slightly smoothed the T_{eff} for the fainter stars in our sample by small amounts to ensure that stars at the approximately same evolutionary stage have the approximately the same stellar parameters.

Once an initial guess at T_{eff} has been established from a broad band color, it is possible with minimal assumptions to evaluate $\log(g)$ using observational data. The adopted distance modulus, initial guess at T_{eff} , and an assumed stellar mass (we adopt $0.8 M_{\odot}$ for the stars in the M5 sample) are combined with the known interstellar absorption, the predictions of the model atmosphere grid for bolometric corrections as well as a broad band observed V mag to calculate $\log(g)$. An iterative

scheme is used to correct for the small dependence of the predictions of the model atmosphere grid on $\log(g)$ itself. Rapid convergence is achieved.

It is important to note that because of the constraint of a known distance to M5, the uncertainty in $\log(g)$ is small, ≤ 0.1 dex when comparing two members of M5. Propagating an uncertainty of 15% in the cluster distance, 5% in the stellar mass, and a generous 3% in T_{eff} , and ignoring any covariance, leads to a potential systematic error of ± 0.2 dex for $\log(g)$.

5.1. The Spectroscopic Excitation Temperature

The excitation temperature (a spectroscopic measure of T_{eff}) of a star can be determined from the observed spectrum by requiring the derived abundance of an ion with many observed lines covering a wide range of lower excitation potential χ to be independent of χ . This technique can be applied to 19 of our stars where we have detected Fe I lines with sufficient range in χ . For the determination of the excitation temperature we use “the weak line set” of Fe I lines to ensure that the resulting Fe abundance and derived spectroscopic T_{eff} will be only weakly dependent on the choice of microturbulent velocity. We find that the spectroscopic T_{eff} is in good agreement with the derived photometric T_{eff} , as shown in Figure 2. The filled circles show the adopted T_{eff} and the open circles show the original T_{eff} , before smoothing the photometric result, as described before. The solid line in Figure 2 indicates the ideal case when the spectroscopic and the photometric T_{eff} are equal. The scatter around the solid line is about 130 K, which is comparable to the error of the photometric T_{eff} given above.

5.2. The Microturbulent Velocity

The microturbulent velocity (ξ) of a star can be determined spectroscopically by requiring the abundance to be independent of the strength of the lines. We apply this technique for the “the weak line set” of Fe I lines. Only 16 of our stars have enough weak Fe I lines to derive ξ spectroscopically. The relationship between the determined ξ and the photometric T_{eff} is shown in Figure 3. The solid line corresponds to a linear least squares fit to the data, given by:

$$\xi = 4.08 - 5.01 \times 10^{-4} \times T_{eff}$$

The scatter around the solid line is about 0.3 km s^{-1} , which is a reasonable estimation of the error in ξ . For the rest of the analysis, we adopt for each star the ξ computed from the ξ - T_{eff} fit. The microturbulent velocity used for each star in our sample in M5 is listed in Table 4. Unless otherwise specified, we use in our analysis the set of all the good atomic lines for each ion as defined in §3.

6. RESULTS

Given the derived stellar parameters from Table 4, we determined the abundances using the equivalent widths obtained as described above. The abundance analysis is carried out using a current version of the LTE spectral synthesis program MOOG (Sneden 1973). We employ the grid of stellar atmospheres from Kurucz (1993a) with a metallicity of $[\text{Fe}/\text{H}] = -1.0$ dex to compute the abundances of O, Na, Mg, Si, Ca, Sc, Ti, V, Cr, Mn, Fe, Co, Ni, Cu, Zn, Zr, Ba, La, and Eu using the four stellar atmosphere models with the closest T_{eff} and $\log(g)$ to each star’s parameters. The abundances were interpolated using results from the closest stellar model atmospheres to the appropriate T_{eff} and $\log(g)$ for each star. We adopt a minimum uncertainty of 0.05 dex in abundance ratios ($[\text{X}/\text{Fe}]$ or $[\text{Fe}/\text{H}]$) for ions with less than 10 detected lines in a star, with the minimum lowered to 0.03 dex for ions with more than 10 measured lines in a given star. If only one line of an ion is detected in a particular star, an uncertainty of 0.10 dex is adopted. Our final results are not sensitive to small changes in the metallicity of the model atmosphere (see below).

6.1. The Iron Abundance

The derived abundance $[\text{Fe}/\text{H}]$ from Fe I lines for each star in our M5 sample is listed in column 3 of Table 5a and plotted against the photometric T_{eff} in the top panel of Figure 4. T_{eff} is used for the x-axis as a convenient parameter for characterizing the position of the stars in the color-magnitude diagram as it ranks the stars in luminosity. The errors listed in column 3 of Table 5a correspond to the larger of the statistical uncertainty, given by the standard deviation of the iron abundance from different lines divided by the square root of the number of lines of Fe I used for a particular star, or a minimum values based on the number of detected lines specified above. These errors are lower limits to the actual uncertainties in the abundances, since they do not include uncertainties due to the stellar parameters nor any systematic effects that might be present.

We evaluate the sensitivity of $[\text{Fe}/\text{H}]$ derived from Fe I lines with respect to small changes in the equivalent widths and the stellar parameters in three cases 4250/1.5/1.8, 5000/3.0/1.5 and 6000/4.0/1.0, where the three numbers correspond to $T_{eff}/\log(g)/\xi$. We estimated the error in the W_λ to be 10% for all the lines. The results are listed in Table 6, where the range adopted for each parameter is representative of its uncertainty. Our determination of $[\text{Fe}/\text{H}]$ from Fe I lines is most sensitive to errors in W_λ (a change of ~ 0.1 dex for a 10% error in the W_λ), and has minimal sensitivity to the choice of metallicity of the model atmosphere for plausible changes in $[\text{Fe}/\text{H}]$ (± 0.2 dex). The solid line, shown in the top panel of Figure 4, is a linear fit (weighted by the errors) to $[\text{Fe}/\text{H}]$ versus T_{eff} . The slope of the fit is $(+9.1 \pm 5.0) \times 10^{-5}$ dex/K, which is consistent with $[\text{Fe}/\text{H}]$ being constant, independent of T_{eff} (ie, of luminosity or equivalently position in the color-magnitude diagram), within a 2σ level. The mean $[\text{Fe}/\text{H}]$ weighted by the errors of all 25 stars is -1.30 ± 0.02 , in very good agreement with earlier determinations (Sneden *et al.* 1992; Shetrone 1996; Ivans *et al.* 2001).

The determinations of $[\text{Fe}/\text{H}]$ from Fe II lines are listed in column 5 of Table 5a and plotted against the photometric T_{eff} in the bottom panel of Figure 4. The errors listed in column 5 of Table 5a correspond to the larger of the statistical uncertainty or to the minimum uncertainty specified above based on the number of detected lines. We evaluate the sensitivity of $[\text{Fe}/\text{H}]$ derived from Fe II lines with respect to small changes in the equivalent widths and the stellar parameters in the same manner as the sensitivity of $[\text{Fe}/\text{H}]$ from Fe I lines. The results are listed in Table 6, where the range adopted for each parameter is representative of its uncertainty. We see a stronger sensitivity on the stellar parameters from the Fe II lines than from the Fe I lines. The $[\text{Fe}/\text{H}]$ determination from Fe II lines is most sensitive to the systematic error in $\log(g)$ (note that the internal uncertainty in $\log(g)$ is smaller, ~ 0.1 dex), as well as to T_{eff} among the coolest M5 giants. The sensitivity on the choice of metallicity of the model atmosphere is again small for reasonable changes in metallicity. The solid line, shown in the bottom panel of Figure 4, is a linear fit weighted by the errors of $[\text{Fe}/\text{H}]$ versus T_{eff} . The slope of the fit is $(+1.2 \pm 0.5) \times 10^{-4}$ dex/K, which is essentially identical to the small, not statistically significant slope obtained from the Fe I lines. The mean $[\text{Fe}/\text{H}]$ weighted by the errors for the 17 M5 stars with detected Fe II lines is -1.28 ± 0.02 , in very good agreement with our result from Fe I lines and earlier determinations (Snedden *et al.* 1992; Shetrone 1996; Ivans *et al.* 2001).

The iron abundance could be affected by departures from LTE. The main NLTE effect in late-type stars arises from overionization of electron donor metals by ultraviolet radiation (Auman & Woodrow 1975). Gratton *et al.* (1999) and Thévenin & Idiart (1999) studied NLTE effects in Fe abundances in metal-poor late-type stars. Gratton *et al.* (1999) found that NLTE corrections for Fe lines are very small in dwarfs of any T_{eff} , and only small corrections (< 0.1 dex) are expected for stars on the red giant branch. Thévenin & Idiart (1999) found that NLTE corrections become more important as $[\text{Fe}/\text{H}]$ decreases, being about 0.2 dex for stars with $[\text{Fe}/\text{H}] \sim -1.25$ dex, and that ionized lines are not significantly affected by NLTE. Very recently, Gehren *et al.* (2001) and Gehren, Korn & Shi (2001) have carefully calculated the kinetic equilibrium of Fe, and present in Korn & Gehren (2002) a critique of earlier calculations. They suggest non-LTE corrections intermediate between the above sets of values are appropriate for Fe I.

One way to explore possible NLTE effects present in our data is by comparing the results from Fe I and Fe II lines. The mean difference between $[\text{Fe}/\text{H}]$ from Fe II and Fe I lines is 0.02 ± 0.18 . The slope of the relationship between $([\text{Fe}/\text{H}]_{\text{FeII}} - [\text{Fe}/\text{H}]_{\text{FeI}})$ vs. T_{eff} is $(+0.6 \pm 1.0) \times 10^{-4}$ dex/K, which is nearly flat. We conclude that NLTE effects are negligible in our iron abundance determination, with a maximum change of 0.12 ± 0.2 dex in the Fe ionization equilibrium from the tip of the RGB to the main sequence turnoff in M5.

6.2. Abundance Ratios

The abundance ratios, with the exception of $[\text{O}/\text{Fe}]$, $[\text{Si}/\text{Fe}]$ and $[\text{Zn}/\text{Fe}]$, are computed using the iron abundance from Fe I lines and our solar abundance ratios from Table 3. Given their high

excitation potentials, the abundance ratios for the Si I and Zn I lines were computed using the $[\text{Fe}/\text{H}]$ from Fe II lines. In the T_{eff} range of our sample of stars in M5, most of the iron is in the form of Fe II and most of the oxygen is in the form of O I, so both species behave similarly for small changes in the atmospheric parameters. For this reason, we computed the abundance ratio of O using the Fe II lines as well. The computed abundance ratios are listed in Tables 5a - 5d. The error listed in Tables 5a - 5d for each ion corresponds to larger of the statistical uncertainty in the mean abundance for the lines of that ion detected in a particular star, i.e. to the standard deviation within our sample of stars divided by the square root of the number of stars for which an abundance was derived for that ion, or to the minimum uncertainty specified above, depending on the number of detected lines.

The O lines were detected in nine of our M5 stars; we provide constraining upper limits on their equivalent widths in other six stars. Among the nine stars with clear detections, we were able to measure both the permitted and forbidden lines in five of them. We find no significant difference between the oxygen abundance derived from permitted and forbidden lines; the $[\text{O}/\text{Fe}]$ listed in Table 5a corresponds to the average results from all the lines detected in each star.

In M71, however, (see §3 of Ramírez & Cohen 2002) we did see a difference between the O abundance deduced from the permitted and from the forbidden lines. R. P. Kraft suggested to us that this might be the consequence of adoption of a reddening value for M71 which is slightly too small. (We used $E(B-V)=0.25$ mag.) This would result in an underestimation of T_{eff} for each M71 star. An increase in the reddening for M71 of only 0.03 mag would produce a change of $\approx 100\text{K}$ in the resulting T_{eff} obtained from the broad band colors $V - I$, $V - J$ and $V - K$. The high excitation potential of the permitted O lines leads to a very high sensitivity to T_{eff} (see Table 6). We have checked that a 100K increase in T_{eff} will in fact eliminate the trend displayed in Figure 1 of Ramírez & Cohen (2002) and produce approximate agreement between the two independent determinations of the O abundance for each star in our sample in M71 for which both permitted and forbidden O lines could be measured. If one chooses to adopt this higher value for the reddening of M71, small changes in the abundance ratios for the M71 stars then follow, which are given in Table 6 of Ramírez & Cohen (2002). At present we lack an accurate determination of the reddening of M71, which might in principle be obtained directly from high precision spectra of the brighter M71 stars without recourse to photometry. Fortunately, the reddening to M5 is much smaller.

The Na D lines were detected in all 25 stars in our sample. Given the low reddening of M5, the stellar Na D lines are relatively free of contamination by interstellar features, and the v_r of M5 shifts the night sky emission lines away from the Na D lines of the cluster stars. Thus the Na D lines could be and were included in the analysis. (This was not possible for M71.) We compare the resulting abundances for the 20 stars where both the Na D lines and the 5682,5688 Å Na doublet were detected. There is a correlation between the sodium abundance derived from the D lines and the one derived from the weak Na lines which does not quite correspond to the desired one of equality. To be consistent, the sodium abundance derived from the D lines was put on the same scale as the sodium abundance derived from the other Na lines, before taking the average.

The spectra of the six main sequence stars in our sample in M5 do not have high signal-to-noise ratios and the lines are in general weak. In a few cases where no line of an ion could be detected in any individual spectrum, we summed the spectra, and this enabled detection of a small number of additional lines. This was done for the O I triplet, the Mg I line at 5528Å, and two Sc II lines. Their equivalent widths and determined abundance ratios are listed in Tables ?? and 5a – 5b, respectively, under the entry "<MS>". In each of these cases, the temperature sensitivity of the lines increases their strength in these hotter low luminosity M5 stars.

The abundance ratios for each star in our M5 sample are plotted against the photometric T_{eff} in Figures 5 to 9. The error bars shown in Figures 5 to 9 are those described above. The solid line, shown in Figures 5 to 9, is a linear fit weighted by the errors of the respective abundance ratio versus T_{eff} . The dashed line shown in these figures indicates the mean abundance ratio and its respective error plotted as an error bar at 4000 K. In the top panel of Figure 5 the arrows correspond to the upper limit in [O/Fe] for six stars in our sample. An open triangle indicates the mean abundance measured in the summed spectrum of the six main sequence stars.

We estimate the sensitivity of abundances with respect to small changes in the equivalent widths and the stellar parameters in the same manner as the sensitivity of [Fe/H] from Fe I lines. The results are listed in Table 6, where the range adopted for each parameter is representative of its uncertainty. The W_λ of the lines of Ti I, V I and Zr I have the strongest dependence on T_{eff} as most of the detected lines from these neutral ions have low excitation potentials. Due to its strong lines, Ba II has the strongest dependence on ξ .

The mean abundance ratios and their errors are listed in Table 7. The error of the mean for an element X corresponds to the standard deviation of the abundance ratio $[X/Fe]$ of the sample of stars in which lines of X were detected, divided by the square root of the number of such stars. The error of the mean computed this way represent the formal statistical uncertainty in the mean abundance considering only the internal errors; it does not include any possible systematic errors that may arise during the analysis. The standard deviation about the mean abundance ratio, σ_{obs} , is a measure of the scatter of the abundance ratio for a particular ion within the sample of M5 stars. In order to quantify the abundance ratio variations within our sample of M5 stars we have to compare the measure of the scatter with the predicted error from the stellar parameters and the measurement of the W_λ . We estimated the predicted error, σ_{pred} , in the same manner as in Ramírez & Cohen (2002). Our σ_{pred} ignores covariance among the error terms, which is discussed in detail by Johnson (2002). She shows that these additional terms are fairly small, and will be even smaller in our case, as we have determined $\log(g)$ using cluster distances rather than through the ionization equilibria of Fe. The general small trends seen in Figures 5 to 9 of $[X/Fe]$ slightly increasing toward cooler T_{eff} , a trend also seen in our analysis of M71 (Ramírez *et al.* 2001; Ramírez & Cohen 2002), may result from ignoring the covariance terms (see Johnson 2002). The predicted errors for each ion are listed in column 5 of Table 7.

A summary of the abundance ratios for our M5 sample is shown in Figure 10. The results for

each element are depicted as a box plot defined by Tukey (1977) (see also Cleveland 1993). The central horizontal line in each box is the median abundance ratio for all the M5 stars included, while the bottom and the top shows its inter–quartile range, the vertical lines coming out of the box mark the position of the adjacent points of the sample, and the outliers are plotted as open circles. The boxes drawn with dotted lines correspond to elements with abundances computed from only one line in each star and hence are more uncertain. The thick line on the left side of the box is the predicted 1σ rms error scaled to correspond to the $\pm 25\%$ inter–quartile range. Figure 10 suggests that the element where we are most likely to see star-to-star variations in our M5 sample is Na; these variations were in fact detected and will be discussed in detail in §7.5.

7. DISCUSSION

7.1. [Fe/H] and Diffusion of Heavy Elements

Our [Fe/H] abundance results provide further evidence that the iron abundance, derived from both Fe I and Fe II lines, is independent of T_{eff} , and equivalently luminosity, within the globular cluster M5, from the top of the giant branch to near the main sequence. Our result in M5 is in agreement with our previous analysis of a sample of M71 stars covering a similar range in luminosity (Ramírez *et al.* 2001). The work of Gratton *et al.* (2001) also supports our [Fe/H] abundance result. They presented abundances from high dispersion spectra from the VLT of stars in NGC 6397 and NGC 6752, finding that [Fe/H] obtained for stars at the base of the subgiant branch agrees within a few percent with the [Fe/H] obtained for stars at the main sequence turnoff. Our results, in both M71 and M5, and those of Gratton *et al.* (2001), appear to be in disagreement with inhomogeneities in [Fe/H] found earlier by King *et al.* (1998) in a small sample of stars in M92. These inhomogeneities may rise from the comparison of data sets analyzed by different groups, who may have determined the stellar parameters and performed the abundance determinations in a different way.

It is clear from helioseismology that atomic diffusion (primarily of He) occurs in the Sun (Basu, Pinsonneault & Bahcall 2000 and references therein). Theoretical investigations of heavy element diffusion in metal poor stars by Michaud, Fontaine & Beaudet (1981), Castellani *et al.* (1997), Salaris, Groenewegen & Weiss (2000), Salaris & Weiss (2001) and Chaboyer *et al.* (2002), among others, suggest that it should be important in metal poor stars at the main sequence turnoff, while at the level of the RGB, the presence of deep surface convection zones should inhibit such processes. Such processes should manifest themselves in most clearly in globular cluster stars due to their old age, giving lots of time for such phenomena to develop, and presumed identical initial chemical composition. They would produce a trend of decreasing abundance with T_{eff} in our data, of an amplitude of ~ 0.2 dex for Fe between the RGB and the main sequence turnoff. The very recent set of models including radiative acceleration as well as gravitational settling by Richard *et al.* (2002) suggest that Fe will rise in metal poor main sequence stars rather than sink, reaching an

excess of a factor of 5 at $[\text{Fe}/\text{H}] = -2.3$ dex just before a star evolves off the main sequence to become a subgiant. Similar large enhancements are predicted for the elements Al to Ca, with the enhancements depending on the age of the star. These theoretical predictions are highly dependent on the details of the modeling of the relevant physical processes.

Although gravitational settling and radiative levitation are clearly detected in hot horizontal branch stars in globular clusters (Behr *et al.* 1999; Behr, Cohen & McCarthy 2000), we continue to see no evidence for such effects in our sample of red giant branch, subgiants, and main sequence globular cluster stars, either in Fe I or in any of the abundance ratios discussed below. To within the precision of our measurements, there is no evidence for any change in abundances with decreasing T_{eff} , i.e. with decreasing luminosity, between the tip of the RGB and the main sequence turnoff. In agreement with other recent studies, particularly that of Gratton *et al.* (2001) and Bonifacio *et al.* (2002) in NGC 6397 and our previous work (Ramírez & Cohen 2002) in M71, we suggest that some process must provide an additional turbulence in low metallicity main sequence stars which inhibits the predicted diffusion of heavy elements.

7.2. Fe-peak elements

The abundance ratios of $[\text{Sc}/\text{Fe}]$, $[\text{V}/\text{Fe}]$, $[\text{Cr}/\text{Fe}]$, $[\text{Mn}/\text{Fe}]$, $[\text{Co}/\text{Fe}]$, and $[\text{Ni}/\text{Fe}]$ follow the behavior of iron as expected, showing no significant trend with T_{eff} , and less or similar scatter around the mean than the predicted error. The exception is Cr I, whose scatter appears unexpectedly large in Fig. 7 and in Table 7. However, although nine lines of this ion were detected in the coolest and most luminous star in our sample, only a single Cr I line could be detected in half of the 14 M5 stars in which we could detect any Cr I lines. The mean abundance ratios of Sc, V, and Ni are consistent with the earlier results of Sneden *et al.* (1992), who analyzed high resolution spectra of 13 giant stars in M5. Our iron-peak abundance ratios are also in agreement with those results obtained by Ivans *et al.* (2001), who analyzed high resolution spectra of 36 giants in M5. A comparison of our abundance ratios with those of these two previous studies for all elements analyzed by them is given in Table 8, which will be discussed in detail in §7.6.

7.3. Neutron capture elements

The abundance ratios of the neutron capture elements, Zr, Ba, La, and Eu, show no significant trend with T_{eff} , and scatter around the mean similar in size to the predicted error. The mean abundance ratios of Ba, La (see §7.6 for details), and Eu are consistent with the earlier results of Ivans *et al.* (2001) listed in Table 8. The abundances of Ba, La, and Eu are overabundant relative to Fe, as is seen in other globular clusters such as M4 (Ivans *et al.* 1999) and M15 (Sneden *et al.* 1997).

The mean $[\text{Ba}/\text{Eu}]$ ratio of -0.64 is consistent with values observed in halo stars of similar

[Fe/H] (Burris *et al.* 2000; Gratton & Sneden 1994). At [Fe/H] ~ -1.3 dex, as reviewed by Burris *et al.* (2000), Ba is a neutron capture element synthesized through s -process reactions that occur mainly in low mass asymptotic giant branch stars, while Eu is exclusively an r -process element.

There are seven stable isotopes of Ba. The Ba isotope ratios in a star depend on the relative contribution of s -process to r -process production⁷. A pure r -process isotopic distribution is assumed by McWilliam (1998), who calculated the hfs splittings we use. As first described by Rutten (1978), ^{135}Ba and ^{137}Ba have components that are shifted both to longer and to shorter wavelengths from the line center, defined roughly by the position of the components from the even isotopes ^{134}Ba , ^{136}Ba and ^{138}Ba . In principle, as suggested by Mashonkina, Gehren & Bikmaev (1999), since the hfs splittings are different for different odd and even isotopes, the deduced abundances from a set of Ba II lines can be used to infer the isotopic distribution and hence constrain the Ba production mechanism(s). In practice, however, as described by Lambert & Allende-Prieto (2002), this is very difficult, even with very high precision spectra with very high signal-to-noise ratio. The issue of the isotopic distribution is not relevant for Eu, where r -process production dominates under all circumstances.

The Zr I lines, which were detected automatically in the three coolest M5 giants, have been checked by hand. The extremely strong Zr I lines in the luminous giant M5 IV-81 are real. In this temperature range, the strength of the Zr I lines increases rapidly as T_{eff} decreases (see Table 6). An overestimate of T_{eff} by 200 K error for this star alone would be required to make the Zr abundance of this star agree with that of the other stars in M5 in which this element was detected. Star IV-81 is included in the sample of Ivans *et al.* (2001), where it is assigned $T_{eff}=3950$ K, 85 K cooler than the effective temperature adopted here. The evidence is inconclusive, but it is interesting to note that we had similar concerns regarding the possible existence of star-to-star variations of Zr in our M71 sample (see Ramírez *et al.* 2001).

7.4. α -elements

We find that the α -elements Mg, Ca, Si and Ti are overabundant relative to Fe. Our mean abundance ratios for Ti and Si are similar to the results of Sneden *et al.* (1992) for 13 M5 giant stars, and also similar to the abundance ratios derived by Ivans *et al.* (2001) for 36 giant stars, as listed in Table 8. Our $\langle[\text{Ca}/\text{Fe}]\rangle$ is higher than the values of Sneden *et al.* (1992) and Ivans *et al.* (2001) The α -element abundance ratios show no significant trend with T_{eff} , and low scatter around the mean.

[Mg/Fe] is known to vary among bright giant stars in some metal poor globular clusters, but no such variation is detected in our sample of stars in M5. In NGC 6752 (Gratton *et al.* 2001),

⁷We ignore two Ba isotopes of very low abundance, (^{130}Ba and ^{132}Ba), which are formed in neither the r nor the s -process.

M13 (Kraft *et al.* 1993; Shetrone 1996) and M15 (Snedden *et al.* 1997), [Mg/Fe] shows a star-to-star range in abundance of more than 1 dex. The mean of the abundance ratio [Mg/Fe] we find in our sample of 25 stars in M5 as well as the scatter about this mean are similar to the results of Ivans *et al.* (2001). Furthermore, our comparison between the observed scatter and the predicted error of [Mg/Fe] given in Table 7 indicates no sign of star-to-star variation of magnesium in M5. [Mg/Fe] showed similar behavior in our previous study sample of M71 stars (Ramírez & Cohen 2002); in particular, no variation in Mg abundance was detected in that cluster either.

7.5. Sodium and Oxygen

The sodium abundance ratios in our sample of stars in M5 behave differently than the abundance ratios of all other elements included in this paper. The observed scatter for [Na/Fe] is more than twice as large as the value of σ_{pred} given in Table 7. This strongly suggests that the scatter in [Na/Fe] shown in Figure 5 arises from star-to-star abundance variations of Na within the 25 stars of our M5 sample. In Figure 11 we compare the strength of the Na I lines between two stars of similar stellar parameters. The star G18450_0453, whose slightly smoothed spectrum is shown as a solid curve, has a high [Na/Fe] (+0.30 dex), and the star G18564_0457, whose slightly smoothed spectrum is shown as a dotted curve, has a low [Na/Fe] (−0.27 dex). These two stars are marked with open squares in the bottom panel of Figure 5. This figure demonstrates again that the higher scatter seen in [Na/Fe] is due to star-to-star abundance variations. Note that both of these stars are red giants more than a magnitude fainter than the horizontal branch.

We have succeeded in reliably detecting O lines in only nine stars of our M5 sample, a reflection of the low metallicity of M5 compared to M71. Among those nine stars, the oxygen abundance ratio is nearly constant and its statistical scatter is similar to the predicted error. The [O/Fe] among those nine stars ranges from 0.37 dex to 0.09 dex, which is significantly smaller than the range from 0.47 dex to −0.55 dex obtained in the analysis of 36 giants from Ivans *et al.* (2001). The O-poor and Na-rich stars found by Ivans *et al.* (2001) are not present in our sample of nine M5 stars, but may be hidden among the six stars with upper limits in [O/Fe] or in the rest of the sample where no useful upper limit could be obtained.

We have summed the spectra of the six main sequence stars to detect more lines at this low luminosity. We were thus able to measure each of the three lines of the O I triplet and derived an abundance from them. The value that we obtain is $[O/Fe]_{MS} = +0.22 \pm 0.07$ (Table 5a), which is very consistent with the mean oxygen abundance ratio of the rest of the M5 sample.

To explore the presence of an anti-correlation between [Na/Fe] and [O/Fe] within our M5 sample, we construct Figure 12, which presents the Na versus O abundance diagram for 15 stars of our sample in M5 where both sodium and oxygen abundance ratios were derived. Our data are indicated by filled triangles and the arrows represent the upper limits for [O/Fe]. The open triangle represent the mean value for the main sequence stars, whose [O/Fe] is obtain through the

equivalent widths measured in the summed spectra and whose $[\text{Na}/\text{Fe}]$ is the average of the values of the main sequence stars derived individually. In view of the large sample of bright RGB stars studied in M4 by Ivans *et al.* (1999), we adopt their results for the observed anti-correlation between Na and O among red giants in this cluster to provide a fiducial line for a visual comparison. The anti-correlation found from their sample is indicated as a dashed line in Figure 12. We find no statistically significant anti-correlation between $[\text{Na}/\text{Fe}]$ and $[\text{O}/\text{Fe}]$ among the nine stars in our sample of M5 with both clear detections of Na I and O I lines. Nevertheless, we cannot rule out its existence when considering that such an anti-correlation might be hidden among the stars with only upper limits for their oxygen abundance ratio.

In Figure 13, we compare our determination of Na and O abundance ratios, in triangles (filled triangles for the M5 RGB and SGB stars and an open triangle for the mean of the main sequence stars), with those from 36 giant stars in M5 from Ivans *et al.* (2001), Shetrone (1996) and Sneden *et al.* (1992), depicted as open squares. The dashed line corresponds to the anti-correlation observed in M4 from Ivans *et al.* (1999), adopted here and in Ramírez & Cohen (2002) as a fiducial line. Our observed range in $[\text{Na}/\text{Fe}]$ is similar to the range observed by these other studies, but our range in $[\text{O}/\text{Fe}]$ is considerably smaller. Note that $\sim 1/3$ of the stars in the sample of Ivans *et al.* (1999) have $[\text{O}/\text{Fe}] \leq 0.0$ dex, while no star in our sample has such a low O, probably because such stars in the luminosity range of our sample would have O I lines that are not detectable at our spectral resolution and signal-to-noise ratio.

7.6. Comparison with Ivans *et al.* (2001)

We summarize here the comparison of our results with those of Ivans *et al.* (2001), which is the most extensive previous high dispersion abundance analysis for M5. Recall that Ivans *et al.* (2001) considered only luminous red giants and AGB stars. There is only one star in common between the two samples, M5 IV-81. We assign to this star a T_{eff} 85 K higher than the value assigned by Ivans *et al.* (2001). Extracting $V - I$ colors from the database of Stetson (2000) for some of the stars in the sample of Ivans *et al.* and then determining T_{eff} with these colors exactly as was done for our sample of M5 stars, we find that at a given V mag along the RGB, the T_{eff} adopted here are about 90 K hotter for stars cooler than 4300 K, with smaller differences for somewhat hotter stars, to the hottest stars in their sample, with $T_{eff} \sim 4700$ K. For a given T_{eff} , we have the same values for $\log(g)$. In view of this close agreement between the stellar parameters adopted for these two studies, we compare the two sets of derived abundances without any adjustments.

The formal statistical uncertainty in the mean abundance of an element in a globular cluster determined by an analysis such as ours is artificially small (< 0.05 dex) as there are many stars in each study, often with many detected lines per star. These small errors are representative of internal errors only, or of comparisons between analyses of different clusters carried out with exactly identical procedures and sources and quality of all data, including both spectroscopic and photometric. However, in comparing between analyses, it is the systematics of small differences in

the temperature scale, the adopted reddening, the adopted atomic data, etc which can introduce much larger differences in the derived abundances. We therefore assign to such comparisons an uncertainty given by $\sigma_c^2 = \sigma(T_{\text{eff}})^2 + \sigma(\log g)^2 + \sigma(\xi)^2 + \sigma([Fe/H]_{\text{model}})^2$, i.e. our normal $1\sigma_{pred}$ uncertainty with the term arising from errors in W_λ set to 0.

Table 8 provides a detailed comparison of the abundance ratios derived here with those of the study of luminous giants in M5 by Ivans *et al.* (2001). In the last column of this table we give the value of σ_c derived for each element from our analysis. Of the 15 ions in common between our work and that of Ivans *et al.* (2001), the only ones with $|[X/Fe](us) - [X/Fe](Ivans)| > 0.16$ dex are O I and Ba II. The difference of +0.24 dex in the mean O abundance presumably reflects our inability to detect weak O lines in the O-poor low luminosity part of our sample in M5, assuming they are actually present there.

We believe that the difference of +0.24 dex in Ba II arises from the difference in the adopted atomic data, isotopic ratios, and Solar abundance between our analysis and that of Ivans *et al.*; the contribution of the last (given in Table 3) is 0.06 dex. The Ba II absorption lines are quite strong among the more luminous RGB stars in M5. They have hyperfine structure, and are quite sensitive to the choice of microturbulent velocity (see Table 6) as well as damping constants.

Given that one believes, based on the evidence presented here and in our earlier work on M71, that the abundances of most, but not all, elements in globular cluster are constant from star to star, one can use the two recent analyses of stars in M5, our analysis and that of Ivans *et al.* (2001), as an end-to-end test of the accuracy of abundance analyses. The two are completely independent, using different model stellar atmospheres grids, different procedures to assign T_{eff} , different ways to measure W_λ and independent choices of atomic data, although the same abundance analysis code. We offer above reasonable explanations to explain the discrepancies in the case of the two elements most divergent between the two analyses. For O I, the explanation involves sample selection and is thus outside the realm of the analysis, while for Ba II it involves the choice of atomic parameters, factors intrinsic to the analysis itself. For the remaining 12 elements in common, Table 8 serves as an interesting example of how well abundance analyses can be carried out on globular cluster stars over a wide range of luminosities in this era of 10-m telescopes. We note the excellent agreement of the Fe abundance, $\Delta[Fe/H] = 0.06$ dex, while for 11 elements in common $\Delta[X/H](us - Ivans) = +0.02 \pm 0.10$ dex

7.7. Comparison with M71

In Figure 14, we provide a comparison between our previous high-resolution abundance analyses of a comparable sample of stars in M71 with the present sample in M5 for every element in common to both analyses. Our previously published M71 abundance ratios have been updated to the same solar abundance scale adopted here for the M5 abundance ratios; see §A and Table 9. The filled squares correspond to our current analysis of M5 stars and the filled triangles to our previous

analysis of M71 stars (Ramírez & Cohen 2002). The error bars indicate σ_c for each abundance ratio. Overall M5 appears to have abundance ratios very similar to those of M71; the mean abundances for each element determined in each globular cluster agree to within the $1\sigma_c$ uncertainties of each measurement for most of the elements displayed. We note that [O/Fe] in M5 appears to be at the top of the range seen in M71, where Ramírez *et al.* (2001) did detect a definite range, again suggesting that in M5 we are failing to detect the full range in O abundance due to weak lines and inadequate precision spectra, and that at least some of our non-detections or upper limits do in fact correspond to low [O/Fe] stars in M5, as were seen by Ivans *et al.* (2001) among the stars near the tip of the RGB.

Nickel and copper show differences in abundance relative to Fe larger than $2\sigma_c$. In each case, the abundance ratio [X/Fe] is smaller in M5 than it is in M71. Nickel is discrepant primarily because its predicted dispersion is so low, 0.05 dex. This occurs because Ni is so similar to Fe in its properties that many errors cancel in forming the abundance ratio [Ni/Fe]. The actual difference of [Ni/Fe](M5-M71) is only -0.13 dex. The abundance of Cu is based on single line which has complex hyperfine structure that might not have been modeled correctly.

The mean abundances deduced from lines of Ba II differ between M71 and M5 by an amount larger than 0.2 dex, but smaller than $2\sigma_c$. There are three reasonably strong Ba II lines used for both the M5 and M71 stars, which makes this perhaps the most credible of the proposed differences between abundance ratios in our sample of stars M71 and in those of M5. This might be related to the dependence with metallicity of the production of *s*- and *r*-process elements (Snedden *et al.* 2001). More likely, however, it too is a reflection of difficulties in the two analyses. The Ba absorption lines tend to be quite strong, hence the choice of damping constants is important. They also have hyperfine structure whose pattern depends on the relative abundances of the various stable isotopes of Ba, which might vary depending on how the Ba is produced. As shown in Table 6, σ_c is large because of the high sensitivity of Ba II lines to changes in v_t . It is interesting to note that the [Ba/Fe] deduced by Ivans *et al.* (2001) for the luminous giants in M5 is close to that we derive for M71, where the Ba II lines are stronger.

If we were to believe that the Ba abundance difference between M5 and M71 is real, we should see a similar difference in the La abundance, as La is also a primarily a *s*-process element at this metallicity. The La abundance, which is based on three weak lines, is from our work identical in M5 and in M71, suggesting that the apparent difference in the Ba abundance between the two clusters is not real.

Some of the well known trends characteristic of halo star abundances as reviewed by McWilliam (1997), such as the overabundance of $[\alpha/\text{Fe}]$ in metal poor stars, are easily seen in Figure 14.

8. Overview and Future Directions

Now that we have completed a detailed abundance analysis for a large sample of stars from the RGB tip to near the main sequence in two globular clusters, we look back to summarize the main trends we have seen, offer some brief remarks in some cases on the possible causes, and some comments on future direction.

First we focus on the fact that for most elements, no star to star scatter in abundance is seen which is larger than that expected from the errors in the observational data and in the analysis. For ions with multiple detected lines, this is a tight constraint, sometimes less than 0.05 dex and often less than 0.1 dex. For this same set of elements, there are no trends of abundance ratios varying with T_{eff} or luminosity within either of these two globular clusters larger than $\pm \sim 0.1$ dex for the better studied elements. Furthermore, with the minor caveats noted in §7.7, there are no substantial changes (> 0.2 dex) in the abundance ratios between M71 and M5 even though M5 is a factor of 4 more metal poor.

In addition to their implications for the formation of globular clusters, a subject we defer to the end of this series of papers, these observational facts provide strong limits for the potential presence and strength of diffusion processes in the atmospheres of globular cluster stars, as discussed in detail in §7.1. The results for Fe (with two ions with multiple detected lines in most stars), and for other elements as well, constrain the amplitude of non-LTE effects (see §6.1).

Both diffusion and non-LTE are expected to produce larger perturbations at lower metallicity. We now have a well understood analysis procedure, which we have verified from end to end through comparison of our results with those of an independent analysis of much brighter stars in M5 by Ivans *et al.* (2001). We are now ready to move to the extremely metal poor globular clusters, as we intend to do in the next papers in this series, with confidence in the validity of our work.

Finally, we turn to the even more interesting case of elements which do show star to star variations. We have seen Na, O and Al vary in a correlated manner in M71. In M5, where Al was not observed and detecting variations in O is quite hard due to the very weak lines in the faint low luminosity stars in our sample, we detected Na varying. In neither cluster did we see Mg varying. To first order, these variations have a constant amplitude independent of luminosity. Much more detailed information is available for C and N from study of molecular bands in the spectra of even larger samples of stars in M5 and in M71 (Cohen 1999; Briley & Cohen 2001; Cohen, Briley & Stetson 2002).

There are many possible explanations for these variations, which we may roughly classify into primordial variations, internal nucleosynthesis within a star plus mixing to the surface of that star, and production of material in some other star which somehow (through stellar winds, supernovae, etc.) then gets accreted onto the star we actually observe. (A variant of the latter scheme involving planets is quite popular lately for some other problems.) These theories each predict the minimum luminosity at which such effects can be detected. For example, if a star is of

such a low mass that Na cannot be produced, irrespective of whether or not mixing of material to the surface is feasible, no Na variations at the stellar surface can be created. A scenario invoking primordial variations within the gas cloud from which the globular cluster formed does not seem to be able to explain why only certain selected elements are varying. Detailed theoretical study of the relevant mechanisms includes meridional mixing (Sweigart & Mengel 1979), turbulent diffusion (Charbonnel 1994, 1995), proton-capture nuclear reactions together with deep mixing (Langer *et al.* 1993; Denisenkov & Denisenkova 1990; Denissenkov & Weiss 1996; Cavallo *et al.* 1998; Weiss *et al.* 2000), and self pollution (Ventura *et al.* 2001).

A key feature is the predicted lowest luminosity (lowest mass) in an old metal poor population (i.e. a globular cluster) at which deep mixing can be effective, which usually is at or near that of the the bump in the luminosity function of the RGB (Bono *et al.* 2001). The location of the bump of the RGB in a cluster of the metallicity of M5 is predicted to be around 0.2 magnitudes above the horizontal branch (Zocalli *et al.* 1999). This is considerably brighter than the stars among which we found variations in O, Na and Mg in M71 or the variations in Na detected here in M5.

A second key feature is the amplitude of and correlation among variations, e.g. in our dataset we find that, in particular, that in M71 Na and O are anti-correlated, while Na and Al are correlated. These are signatures to the process by which this material was synthesized. We suggest that to first order the amplitude of the abundance variations appears to be independent of luminosity, another important clue.

The weight of the evidence is now overwhelming that substantial variations exist in the elements C, N, O, Na and Al well below the cutoff luminosity of the RGB bump. Variations in all of these elements, except perhaps Al, reach to even lower luminosities, below the base of the giant branch to the main sequence in old metal-poor stellar populations. Current theories are hard-pressed to reproduce the trends seen among low luminosity stars in globular clusters in the mounting body of observational data on abundance variations from our own work here and in M71 (Ramírez & Cohen 2002) as well as that of others (47 Tuc by Cannon *et al.* 1998 and NGC 6752 by Gratton *et al.* 2001). We can only hope that continued work in this field, particularly our our upcoming papers on even more metal poor globular clusters, and continued parallel work on variation of the molecular bands in these stars, combined with the continued development of various theoretical aspects of stellar evolution, will lead us to new insights and resolution of these issues.

The entire Keck/HIRES user communities owes a huge debt to Jerry Nelson, Gerry Smith, Steve Vogt, and many other people who have worked to make the Keck Telescope and HIRES a reality and to operate and maintain the Keck Observatory. We are grateful to the W. M. Keck Foundation for the vision to fund the construction of the W. M. Keck Observatory. The authors wish to extend special thanks to those of Hawaiian ancestry on whose sacred mountain we are privileged to be guests. Without their generous hospitality, none of the observations presented herein would have been possible. We acknowledge a special debt to Brad Behr, who participated in the very early stages of this project. We thank Peter Stetson for providing his photometry database

in digital form. We are grateful to the National Science Foundation for partial support under grant AST-9819614 and AST-0205951 to JGC. We thank Jason Prochaska and Andy McWilliam for providing their tables of hyperfine structure in digital form.

A. Updated M71 Abundances

For convenience, we present in Table 9 the updated abundance ratios for M71 after the modifications described here of updating our adopted Solar abundances as described in §4.3 and correcting an error in the transition probability used for the 6497Å line of Ba II in our earlier work on M71 (Ramírez & Cohen 2002). An error in the Ca I damping constants used in our earlier work has also been corrected here.

REFERENCES

- Anders, E. & Grevesse, N., 1989, *Geochim. Cosmochim. Acta*, 53, 197
- Arp, H. C., 1962, *AJ*, 135, 311
- Aresen, A., Bengtsson, A., Hallin, R., Lindskog, J. & Nordland, T., 1977, *Physica Scripta*, 16, 31
- Auman, J. R. & Woodrow, J. E. J., 1975, *ApJ*, 197, 163
- Bard, A., Kock, A., & Kock, M., 1991, *A&A*, 248, 315
- Bard, A., & Kock, M., 1994, *A&A*, 282, 1014
- Basu, S., Pinsonneault, M. H. & Bahcall, J. N., 2000, *ApJ*, 529, 1081
- Baumüller, D., Butler, K., & Gehren, T., 1998, *A&A*, 338, 637
- Behr, B. B., Cohen, J. G. & McCarthy, J. K., 1999, *ApJ*, 517, L135
- Behr, B. B., Cohen, J. G. & McCarthy, J. K., 2000, *ApJ*, 531, L37
- Biémont, E., Baudoux, M., Kurucz, R. L., Ansbacher, W., & Pinnington, E. H., 1991a, *A&A*, 249, 539
- Biémont, E., Grevesse, N., Hannaford, P. & Lowe, R.M., 1981, *ApJ*, 248, 867
- Blackwell, D. E., Petford, A. D., & Shallis, M. J., 1979, *MNRAS*, 186, 657
- Blackwell, D. E., Shallis, M. J., & Simmons, G. J., 1980, *A&A*, 81, 340
- Blackwell, D. E., Petford, A. D., Shallis, M. J., & Simmons, G. J., 1982a, *MNRAS*, 199, 43
- Blackwell, D. E., Petford, A. D., & Simmons, G. J., 1982b, *MNRAS*, 201, 595
- Blackwell, D. E., Booth, A. J., Haddock, D. J., Petford, A. D., & Leggett, S. K., 1986, *MNRAS*, 220, 549
- Bonifacio, P. *et al.*, 2002, *A&A*, 390, 91
- Bono, G., Cassisi, S., Zocalli, M. & Piotto, G., 2001, *ApJ*, 546, L109
- Briley, M. M. & Cohen, J. G., 2001,
AJ, 122, 242
- Buonanno, R., Corsi, C. E. & Fusi Pecci, F., 1981, *MNRAS*, 196, 435
- Burris, D. L., Pilachowski, C. A., Armandroff, T. E., Sneden, C., Cowan, J. J., & Roe, H., 2000, *ApJ*, 544, 302

- Cannon, R. D., Croke, B. F. W., Bell, R. A., Hesser, J. E., & Stathakis, R. A., 1998, MNRAS, 298, 601
- Castellani, V., Ciacio, F., Delg’Innocenti, S. & Fiorentini, G. 1997, A&A, 322, 801
- Cavallo, R. M., Sweigart, A. V., & Bell, R. A., 1998, ApJ, 492, 575
- Chaboyer, B., Fenton, W. H., Nelan, J. E., Patnaude, D. J. & Simon, F. E., 2002, ApJ, 562 521
- Charbonnel, C., 1994, A&A, 282, 811
- Charbonnel, C., 1995, ApJ, 453, L4
- Cleveland, W.S., 1993, *Visualizing Data*, Hobart Press, Summit, New Jersey
- Cohen, J. G., 1999, AJ, 117, 2434
- Cohen, J. G., Frogel, J. A., Persson, S. E. & Elias, J. H., ApJ, 249, 481, 1981
- Cohen, J. G., Behr, B. B., & Briley, M. M., 2001, AJ, 122, 1420
- Cohen, J. G., Briley, M. M., & Stetson, P. B., 2002, AJ, 123, 2525
- Coliss, C. H. & Bozman, W. R., 1962, *Experimental Transition Probabilities for Spectral Lines of Seventy Elements*, NBS Monograph 53, US Government Printing Office
- Cudworth, K.C., 1979, AJ, 84, 1866
- Denisenkov, P. A. & Denisenkova, S. N., SvAL, 16, 275
- Denissenkov, P. A. & Weiss, A., 1996, A&A, 308, 773
- Fuhr, J. R., Martin, G. A., & Wiese, W. L., 1988, J. Phys. Chem. Ref. Data 17, Suppl. 4
- Gehren, T., Butler, K., Mashonkina, L., Reetz, J. & Shi, J., 2001a, A&A, 366, 981
- Gehren, T., Korn, A. J. & Shi, J., 2001b, A&A, 380, 645
- Gratton, R. G. & Sneden, C., 1994, A&A, 287, 927
- Gratton, R. G., Carretta, E., Eriksson, K., & Gustafsson, B., 1999, A&A, 350, 955
- Gratton, R. G., Bonifacio, P., Bragaglia, A., Carretta, E., Castellani, V., Centurion, M., Chieffi, A., Claudi, R., Clementini, G., D’Antona, F., Desidera, S., Francois, P., Grundahl, F., Lucatello, S., Molaro, P., Pasquini, L., Sneden, C., Spite, F., & Straniero, O., 2001, A&A, 369, 87
- Grevesse, N. & Sauval, A. J., 1998, Space Science Reviews, 85, 161
- Gustafsson, B., Bell, R.A., Eriksson, K. & Nordlund, A&A, 1975, A&A, 42, 407

- Harris, W. E., 1996, AJ, 112, 1487
- Holweger, H., Bard, A., Kock, A., & Kock, M., 1991, A&A, 249, 545
- Houdashelt, M. L., Bell, R. A. & Sweigart, A. V., 2000, AJ, 119, 1448
- Ivans, I. I., Sneden, C., Kraft, R. P., Suntzeff, N. B., Smith, V. V., Langer, G. E., & Fulbright, J. P., 1999, ApJ, 118, 1273
- Ivans, I. I., Kraft, R. P., Sneden, C., Smith, G., Rich, R. M., & Shetrone, M., 2001, ApJ, 122, 1438
- Johnson, K. A. & Bolte, M., 1998, AJ, 115, 693
- Johnson, J., 2002, ApJS, 139, 219
- King, J. R., Stephens, A., Boesgaard, A. M., & Deliyannis, C. P., 1998, ApJ, 115, 666
- Korn, A. J. & Gehren, T., 2002, in IAU Symposium 210, *Modelling of Stellar Atmospheres*, Uppsala, June 2002.
- Kraft, R. P., Sneden, C., Langer, G. E., & Shetrone, M. D., 1993, AJ, 106, 1490
- Kraft, R. P., 1994, PASP, 106, 553
- Kurucz, R. L., 1993*a*, ATLAS9 Stellar Atmosphere Programs and 2 km/s Grid, (Kurucz CD-ROM No. 13)
- Kurucz, R. L., 1993*b*, SYNTHE Spectrum Synthesis Programs and Line Data (Kurucz CD-ROM No. 18)
- Lambert, D. L. & Allende-Prieto, C., 2002, MNRAS, 335, 325
- Langer, G. E., Hoffman, R. & Sneden, C., 1993, PASP, 105, 301
- Lawler, J. E., Bonvallet, G. & Sneden, C., 2001, ApJ, 556, 452
- Lawler, J. E., Wickliffe, M. E., den Hartog, E. A. & Sneden, C., 2001, ApJ, 563, 1075
- Martin, G. A., Fuhr, J. R., & Wiese, W. L., 1988, J. Phys. Chem. Ref. Data 17, Suppl. 3
- Mashonkina, L., Gehren, T. & Bikmaev, I., 1999, A&A, 343, 519
- May, M., Richter, J., & Wichelmann, J., 1974, A&AS, 18, 405
- McWilliam, A., 1997, ARA&A, 35, 503
- McWilliam, A., 1998, AJ, 115, 1640
- Michaud, G., Fontaine, G. & Beaudet, G., 1984, ApJ, 282, 206

- Moore, C. E., Minnaert, M. G. J., & Houtgast, J., 1966, *The Solar Spectrum 2935 Å to 8770 Å*, National Bureau of Standards Monograph, Washington: US Government Printing Office (USGPO).
- O'Brian, T. R., Wickliffe, M. E., Lawler, J. E., Whaling, W., & Brault, J. W., 1991, *J. Opt. Soc. Am.*, B8, 1185
- Pinsonneault, M., 1997, *ARA&A*, 35, 557
- Prochaska, J. X., Naumov, S. O., Carney, B. W., McWilliam, A., & Wolfe, A. M., 2000, *ApJ*, 120, 2513
- Ramírez, S. V., Cohen, J. G., Buss, J., & Briley, M. M., 2001, *AJ*, 122, 1429
- Ramírez, S. V. & Cohen, J. G., 2002, *AJ*, 123, 3277
- Rastroguev, A.S. & Samus, N.N., 1991, *Soviet Astron. Lett.*, 17, 388
- Richard, P., Michaud, G., Richer, J., Turcotte, S., Turck-Chieze, S. & Vandenberg, D. A., 2002, *ApJ*, 568, 979
- Rutten, R. J., 1978, *Solar Physics*, 56, 237
- Salaris, M., Groenewegen, M. A. T. & Weiss, A., 2000, *A&A*, 355, 299
- Salaris, M. & Weiss, A., 2001, *A&A*, 376, 955
- Sandquist, E. L., Bolte, M., Stetson, P. B., Hesser, J. E., 1996, *ApJ*, 470, 910
- Schlegel, D. J., Finkbeiner, D. P. & Davis, M., 1998, *ApJ*, 500, 525
- Shetrone, M. D., 1996, *AJ*112, 1517
- Smith, G., 1981, *A&A*, 103, 351
- Smith, G. & Raggett, D. St. J., 1981, *J. Ph. B*, 14, 4015
- Snedden, C., 1973, Ph.D. thesis, Univ. of Texas
- Snedden, C., Kraft, R. P., Langer, G. E., Prosser, C. F., & Shetrone, M. D., 1992, *AJ*, 104, 2121
- Snedden, C., Kraft, R. P., Langer, G. E., Prosser, C. F., & Shetrone, M. D., 1997, *AJ*, 114, 1964
- Snedden, C., Cowan, J. J. & Truran, J. W., 2001, *Astro-ph/0101439*
- Stetson, P. B., Hesser, J. E., Smecker-Hane, T. A., 1998, *PASP*, 110, 533
- Stetson, P. B., Bolte, M., Harris, W. E., Hesser, J. E., van den Bergh, S., Vandenberg, D. A., Bell, R. A., Johnson, J. A., Bond, H. E., Fullton, L. K., Fahlman, G. C. & Richer, H. B., 1999, *AJ*, 117, 247

- Stetson, P. B., 2000, *PASP*, 112, 925
- Sweigart, A. V. & Mengel, J. G., 1979, *ApJ*, 229, 624
- Thévenin, F., 1989, *A&AS*, 77, 137
- Thévenin, F., 1990, *A&AS*, 82, 179
- Thévenin, F. & Idiart, T. P., 1999, *ApJ*, 521, 753
- Tukey, J. W., 1977, *Exploratory Data Analysis*, Addison-Wesley
- Ventura, P., D’Antona, F., Mazzitelli, I. & Gratton, R., 2001, *ApJ*, 550, 65L
- Vogt, S. E. *et al.* 1994, *SPIE*, 2198, 362
- Wallace, L., Hinkle, K. & Livingston, W.C., 1998, N.S.O. Technical Report 98-001, <http://ftp.noao.edu.fts/visatl/README>
- Weise, W. L., Smith, M. W., & Miles, B. M., 1969, *Natl Stand. Ref. Data Ser.*, Natl Bur. Stand. (U.S.), NSRDS-NBS 22, Vol. II
- Weise, W. L., Fuhr, J. R., & Deters, T. M., 1996, *J. Phys. Chem. Ref. Data Monograph No. 7*
- Weiss, A., Denissenkov, P. A., & Charbonnel, C., 2000, *A&A*, 356, 181
- Wolnik, S. J., Berthel, R. O., & Wares, G. W., 1971, *ApJ*, 166, L31
- Zhao, G., Butler, K., & Gehren, T., 1998, *A&A*, 333, 219
- Zocalli, M., Cassisi, G., Piotto, G., Bono, G. & Salaris, M., 1999, *ApJ*, 518, L49

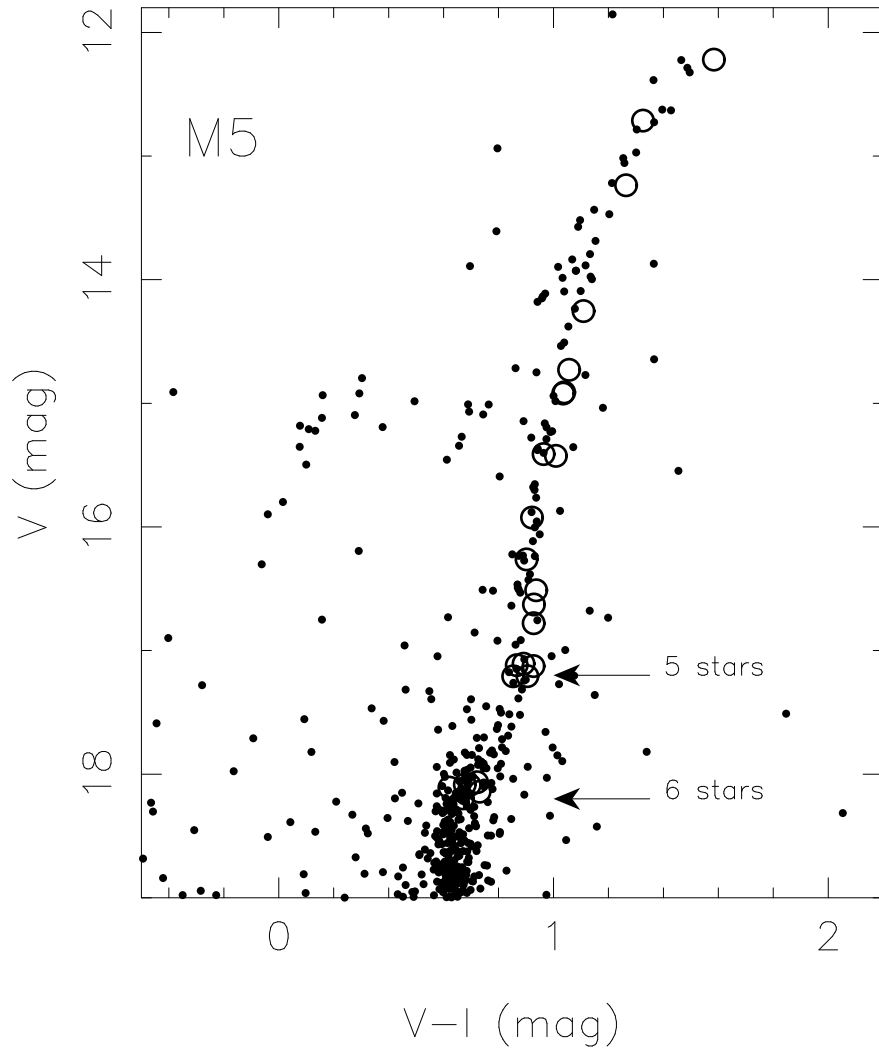


Fig. 1.— HR diagram of M5. The photometry comes from Stetson *et al.* (1998); Stetson (2000). The open circles mark the position of the stars in our M5 sample observed with HIRES (excluding two BHB stars).

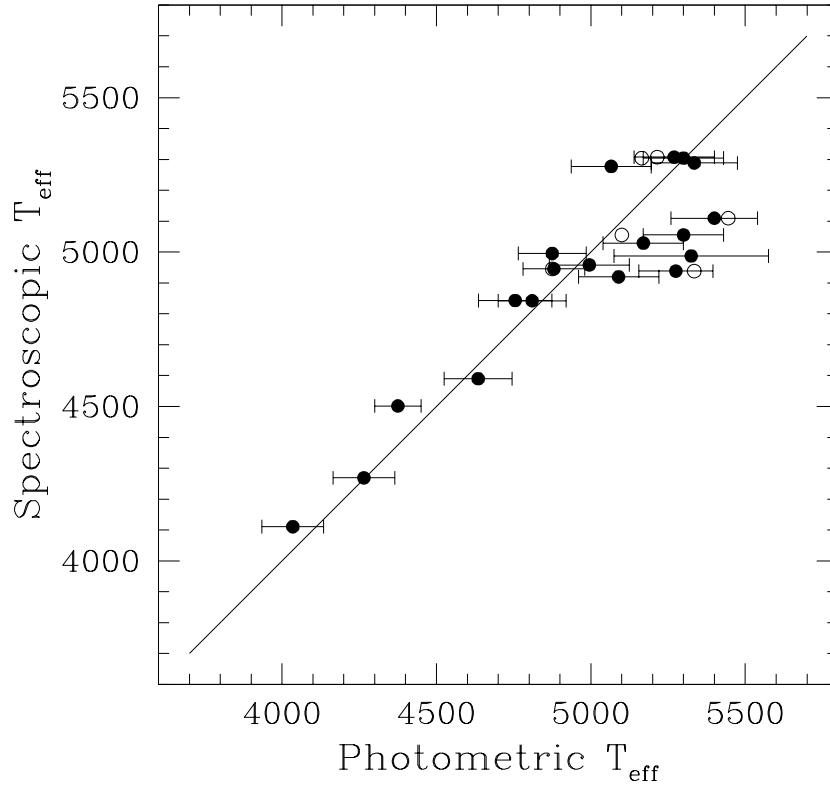


Fig. 2.— Photometric T_{eff} versus spectroscopic (Fe I excitation) T_{eff} for the M5 sample. The filled circles show the adopted T_{eff} and the open circles show the original T_{eff} , before smoothing the photometric result (see text). The solid line indicates the ideal case when the photometric and spectroscopic T_{eff} are equal. The scatter around the solid line is about ± 130 K.

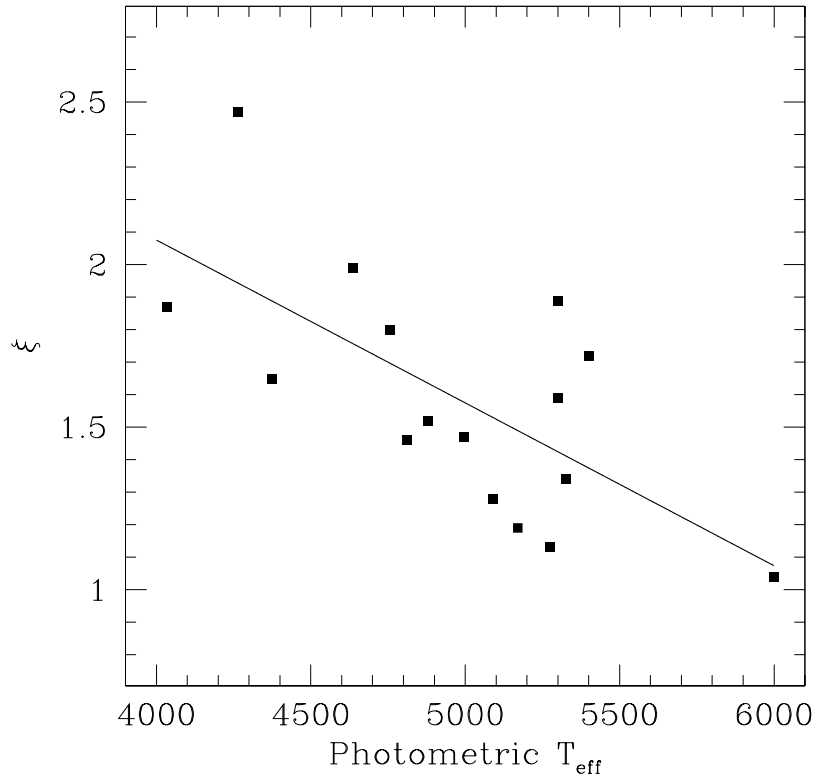


Fig. 3.— ξ determined for the set of weak Fe I lines is shown as a function of T_{eff} . The solid line is the linear fit weighted by the errors. The scatter around the solid line is about ± 0.3 km s⁻¹.

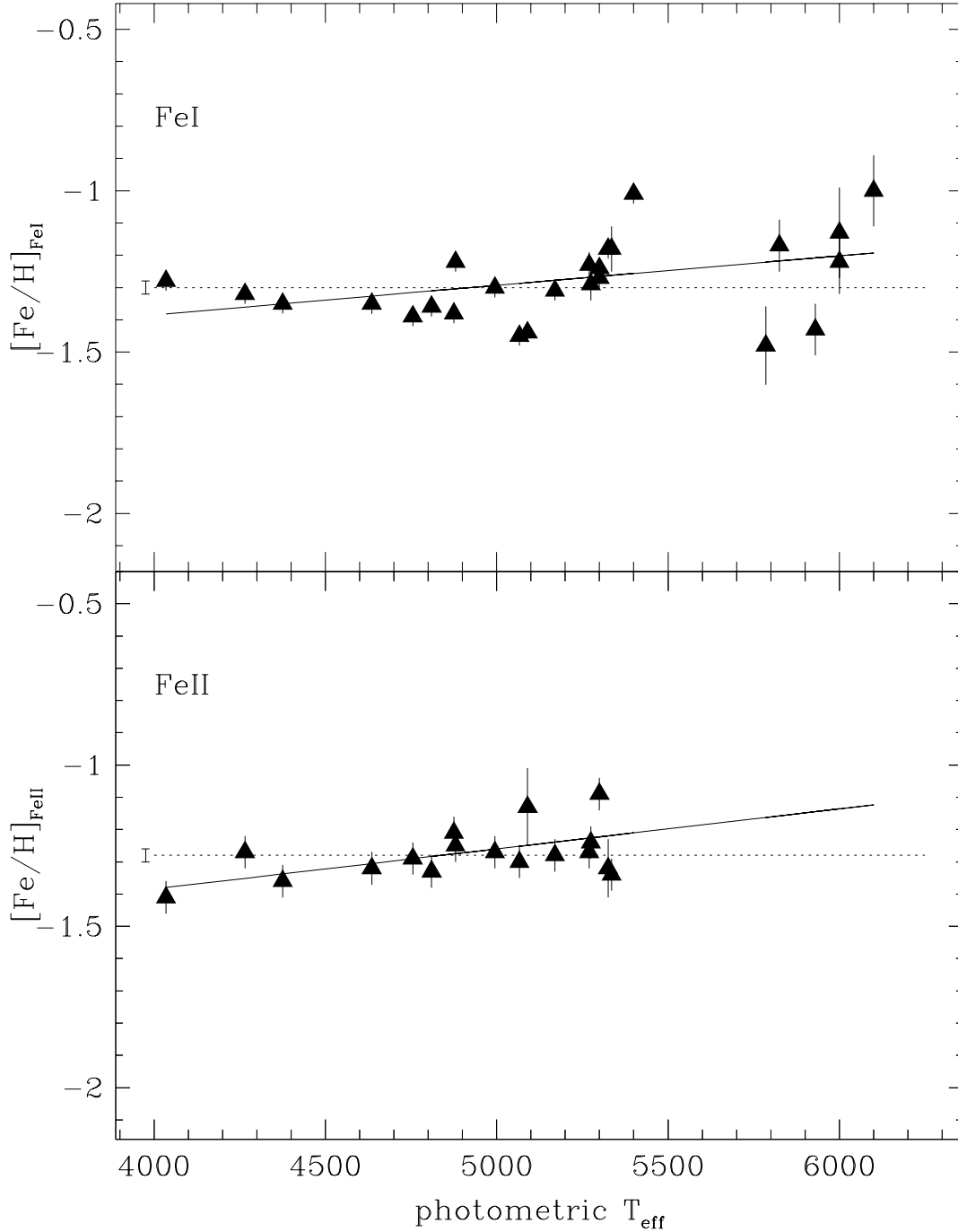


Fig. 4.— [Fe/H] from Fe I (upper panel) and Fe II (lower panel) against photometric T_{eff} . The solid lines are linear fits weighted by the errors. In both cases, [Fe/H] shows no dependence with T_{eff} . The dashed lines indicate the mean [Fe/H] with their respective error plotted as an error bar at 4000 K. Note that $\langle [\text{Fe}/\text{H}](\text{Fe I}) \rangle = -1.30 \pm 0.02$ and $\langle [\text{Fe}/\text{H}](\text{Fe II}) \rangle = -1.28 \pm 0.02$.

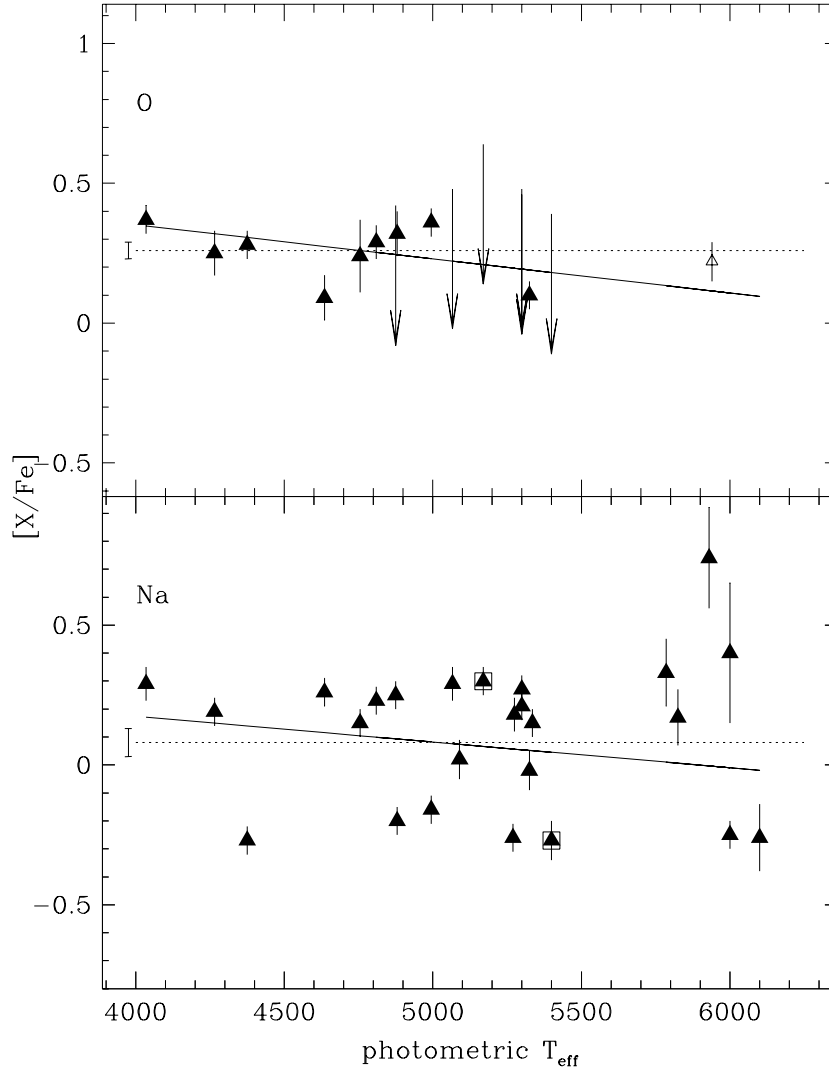


Fig. 5.— Abundance ratios of O and Na with respect to Fe against T_{eff} . The solid line is a linear fit weighted by the errors. The dashed line indicates the mean abundance ratio with its respective error plotted as an error bar at 4000 K. The open triangle corresponds to the abundance determined from the summed spectra of the six main sequence stars. Arrows represent upper limits for the oxygen abundance ratio. Stars G18450_0453 and G18564_0457, part of whose spectra are shown in Figure 11, are marked with open squares in the $[\text{Na}/\text{Fe}]$ panel.

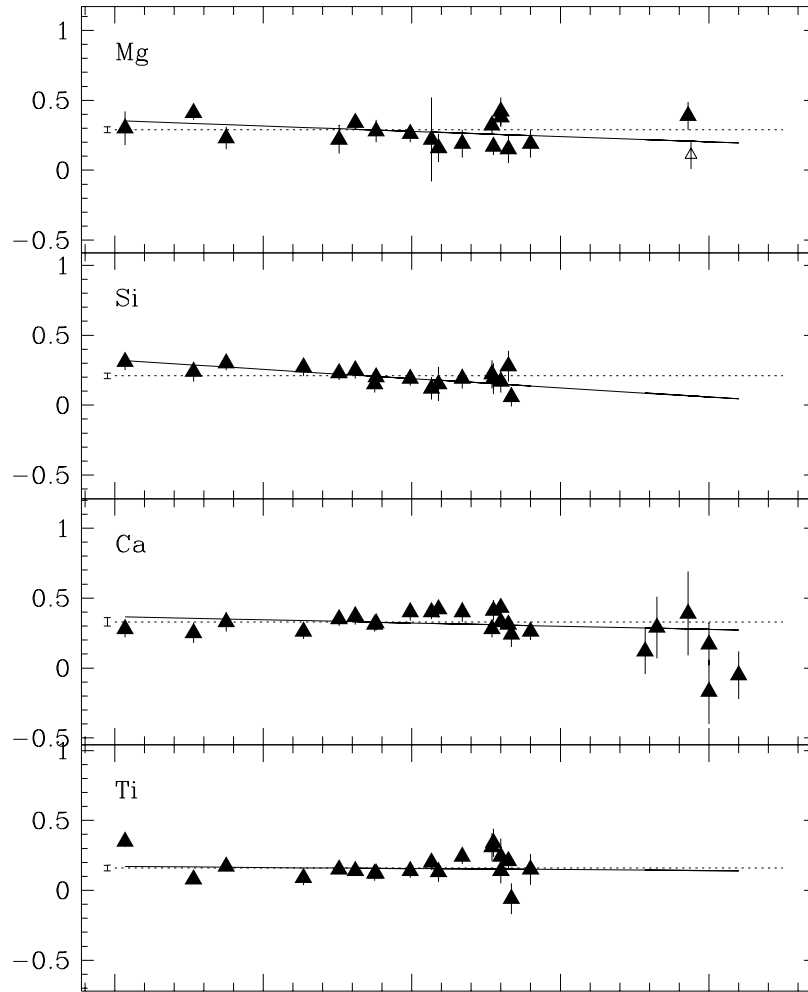


Fig. 6.— Abundance ratios of the α -elements Mg, Si, Ca and Ti with respect to Fe against T_{eff} . The symbols are the same as in Figure 5.

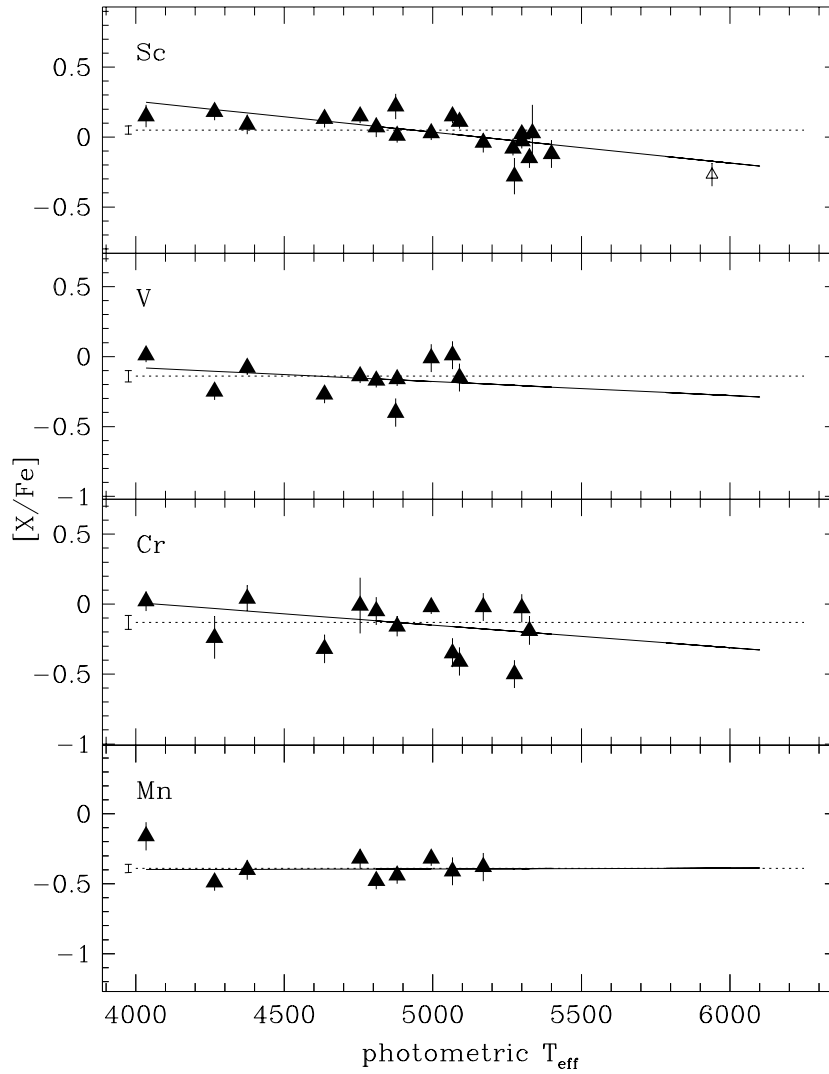


Fig. 7.— Abundance ratios of the iron peak elements Sc, V, Cr, and Mn with respect to Fe against T_{eff} . The symbols are the same as in Figure 5.

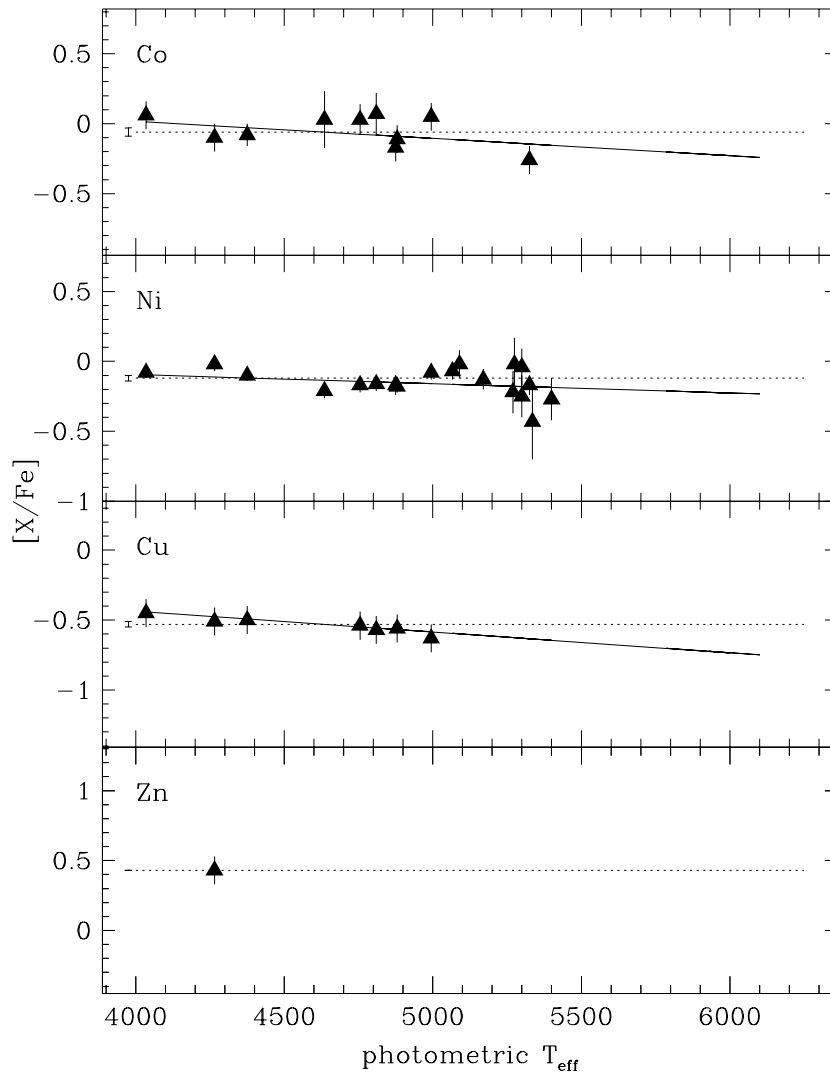


Fig. 8.— Abundance ratios of the iron peak elements Co, Ni, Cu, and Zn with respect to Fe against T_{eff} . The symbols are the same as in Figure 5.

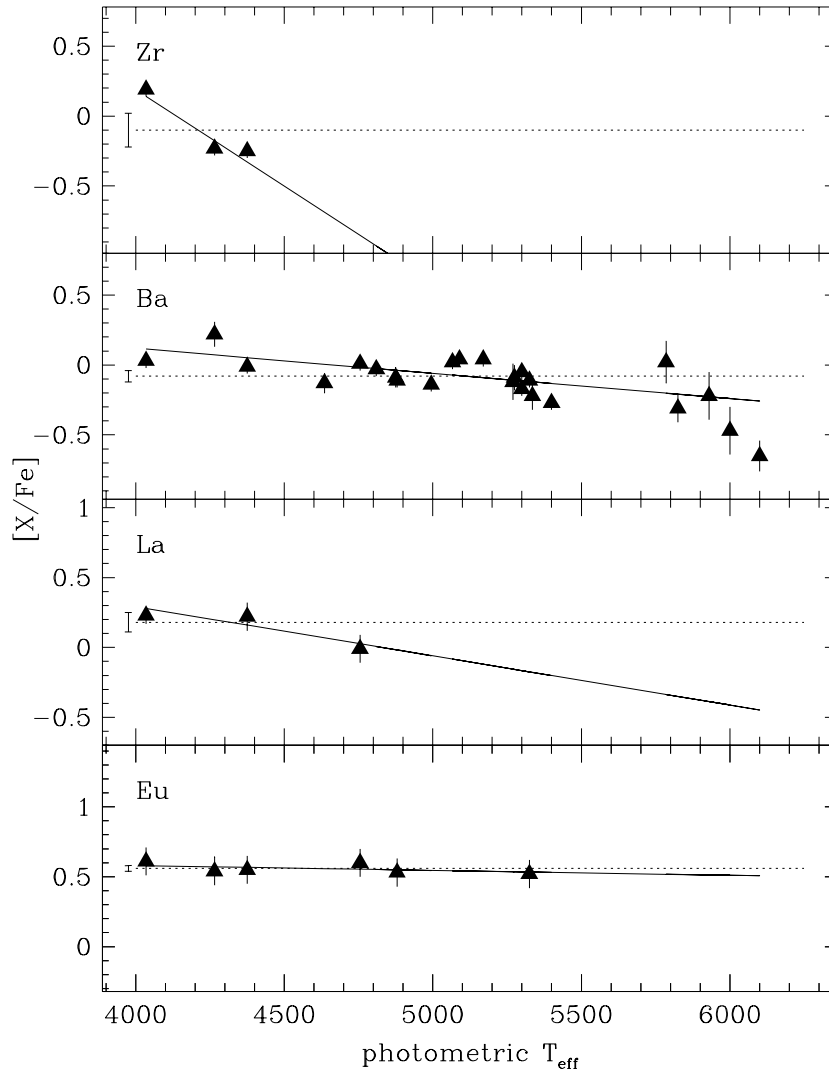


Fig. 9.— Abundance ratios of the neutron capture elements Zr, Ba, La, and Eu with respect to Fe against T_{eff} . The symbols are the same as in Figure 5.

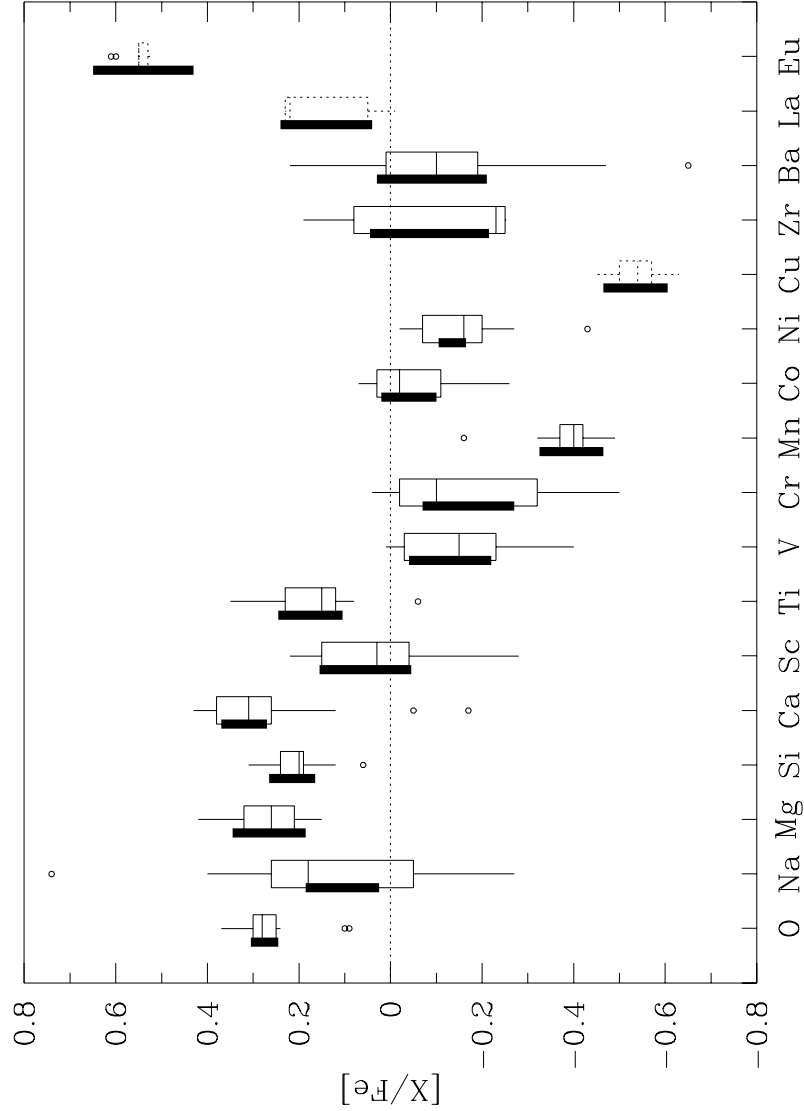


Fig. 10.— Summary of abundance ratios in M5. Each abundance ratio is plotted with a box whose central horizontal line is the median abundance ratio, the bottom and the top shows its interquartile range, the vertical lines coming out of the box mark the position of the adjacent points of the sample, and the outliers are plotted as open circles. Boxes constructed with dashed lines denote elements where only one line per star was observed. The thick line on the left side of the box is the predicted error (expected for the interquartile range) which includes the dependence on the stellar parameters and the equivalent width determination.

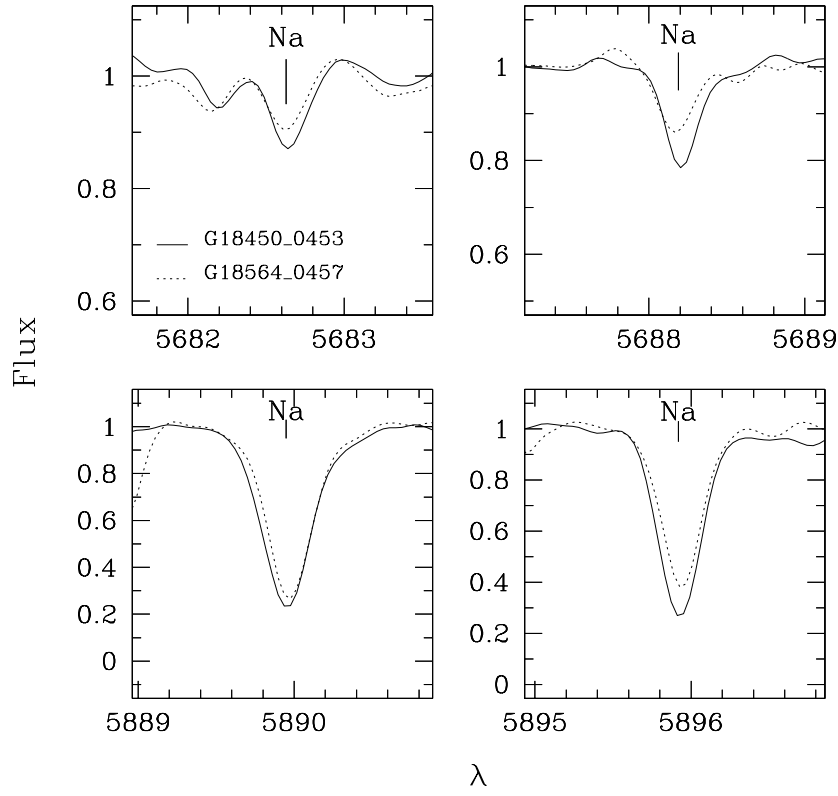


Fig. 11.— Comparison of the strength of four Na I between two stars of similar effective temperatures, G18450_0453 (5170 K, $[\text{Na}/\text{Fe}] = +0.30$) and G18564_0457 (5400 K, $[\text{Na}/\text{Fe}] = -0.27$). The scatter shown by $[\text{Na}/\text{Fe}]$ is due to real abundance variations among stars of similar T_{eff} .

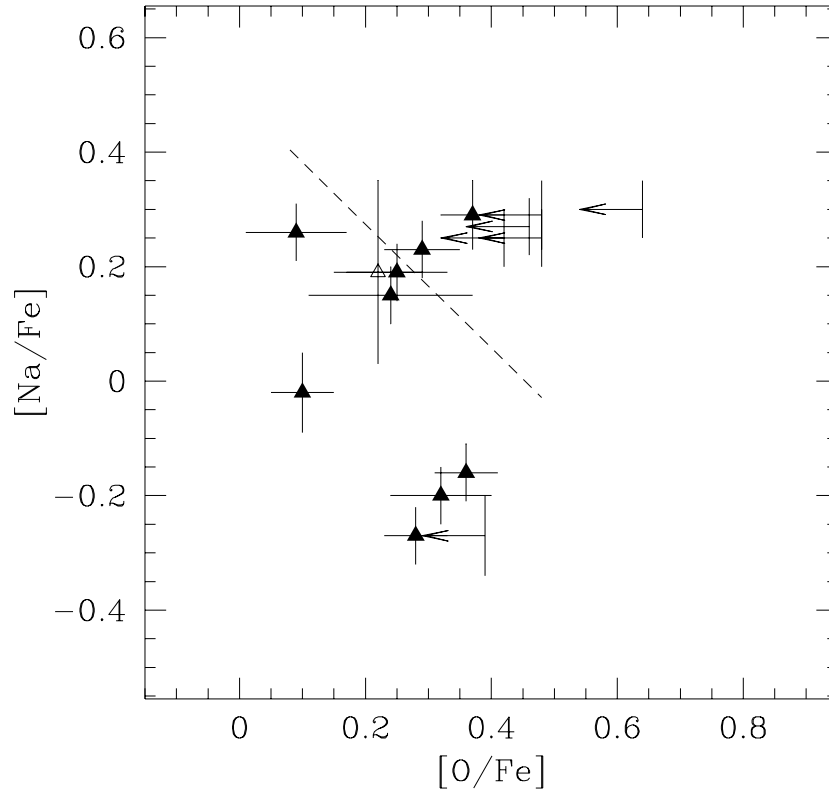


Fig. 12.— $[\text{Na}/\text{Fe}]$ against $[\text{O}/\text{Fe}]$ for our sample of M5 stars. Arrows represent upper limits for the $[\text{O}/\text{Fe}]$ abundance ratio. The open triangle corresponds to the mean abundance of the six main sequence stars. The dashed line corresponds to the Na–O anti-correlation present in M4 from the analysis of Ivans *et al.* (1999), shown as a fiducial line.

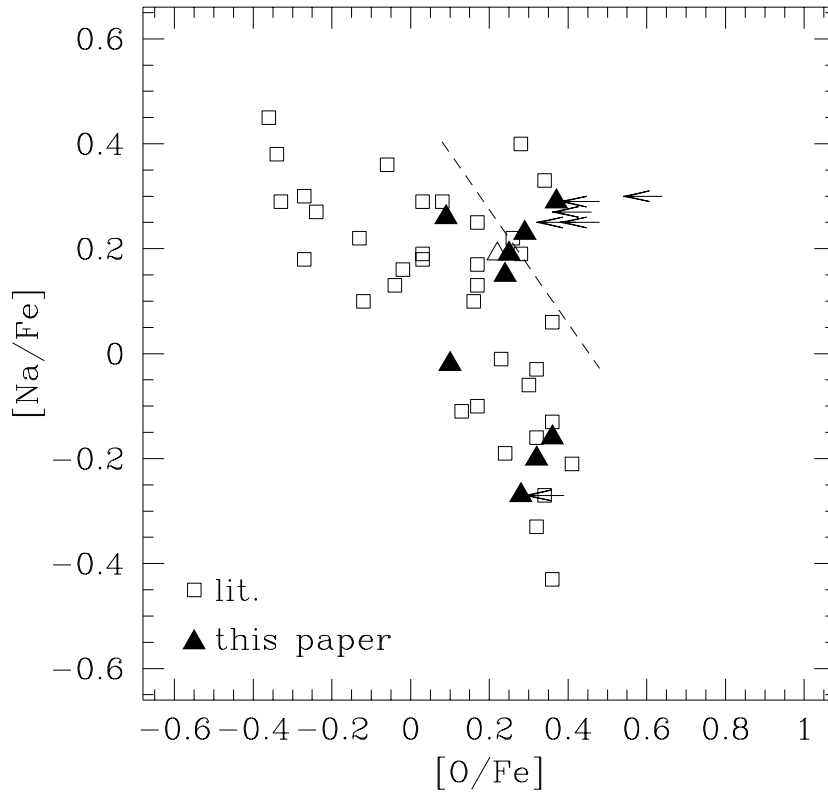


Fig. 13.— $[Na/Fe]$ against $[O/Fe]$ for stars in M5 from our analysis (filled triangles for clear detections, open triangle for mean main sequence stars) and others from the literature (Ivans *et al.* 2001; Shetrone 1996; Sneden *et al.* 1992) (open squares). Arrows represent our upper limits for the $[O/Fe]$ abundance ratio. The dashed line corresponds to the anti-correlation observed in M4 from Ivans *et al.* (1999), shown as a fiducial line.

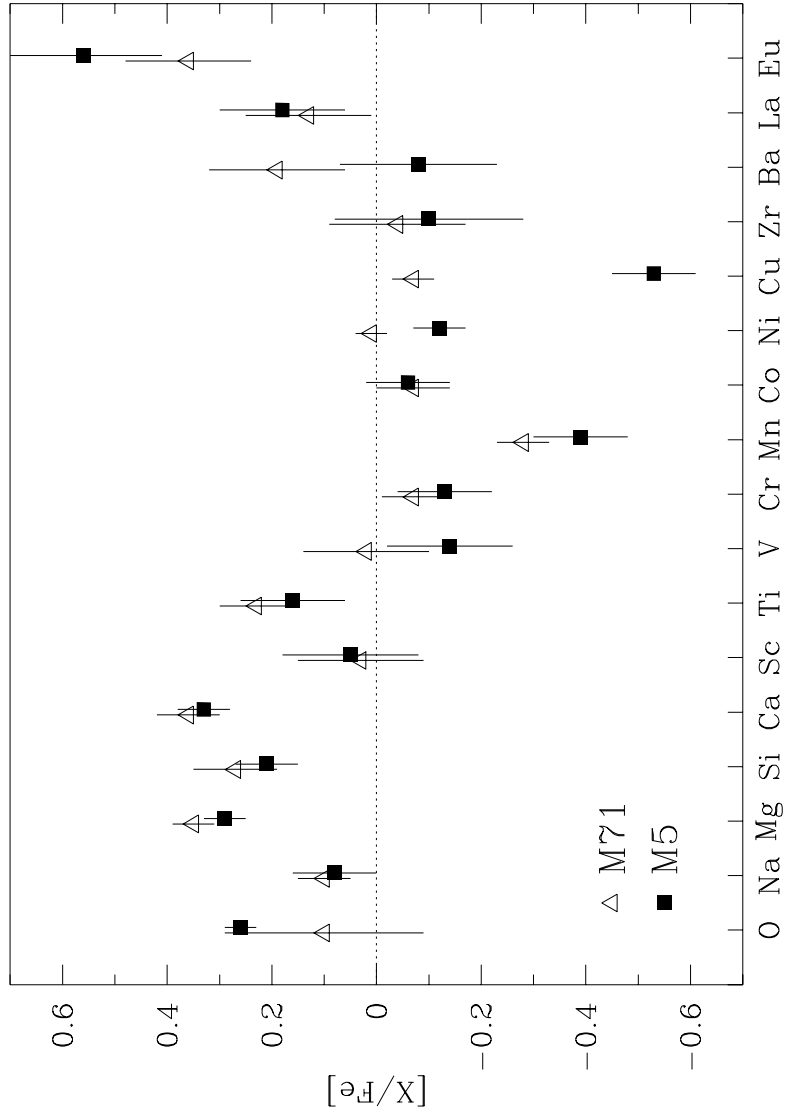


Fig. 14.— A comparison of the abundance ratios for all elements in common between our analysis of similar data for 25 stars in M71 (Ramírez & Cohen 2002), shown by triangles, and in M5 (this paper), shown as squares. The error bars correspond to the σ_c calculated for each cluster.

Table 1. The Sample of Stars in M5.

ID ^a	V (mag)	Date Obs.	Exp. Time (sec)	SNR ^b	v_r (km s ⁻¹)
IV-81	12.22	6/2000	700	> 100	+58.1
IV-59	12.71	6/2000	400	> 100	+59.8
IV-82	13.24	6/2000	700	> 100	+48.1
1-109	14.25	5/2001	1400	> 100	+58.9
1-36	14.73	6/2000	7200	> 100	+60.7
1-31	14.86	6/2000	4800	> 100	+57.3
1-40	14.92	6/2000	3600	> 100	+55.1
G18484_0316	15.41	6/2000	4800	> 100	+55.3
1-110	15.43	5/2001	1400	90	+57.3
G18484_0309	15.93	6/2000	4800	> 100	+58.1
G18450_0453	16.26	6/2000	6000	75	+54.2
1-32	16.51	6/2000	4800	92	+57.9
G18458_0547	16.63	6/2000	7200	89	+50.2
G18447_0453	16.69	6/2000	6000	75	+49.4
G18155_0228	17.11	5/2001	7200	64	+52.0
G18564_0457	17.06	5/2001	7200	64	+53.4
G18445_0448	17.13	6/2000	6000	88	+63.8
G18483_0608	17.21	5/2001	7200	68	+53.6
G18279_0101	17.21	5/2001	7200	66	+53.8
G18569_0455	18.07	5/2001	7200	42	+50.6
G18152_0232	18.09	5/2001	7200	45	+48.6
G18487_0606	18.09	5/2001	7200	43	+54.6
G18172_0750	18.11	5/2001	7200	50	+59.7
G18279_0107	18.14	5/2001	7200	43	+47.6
G18175_0749	18.14	5/2001	7200	41	+56.7

^aIdentifications are from Arp (1962), from Buonanno *et al.* (1981) or are assigned based on the J2000 coordinates, 15 rm rs.s +2 dm dd becoming Grmrss_dmdd.

^bSignal to noise ratio in the continuum near 6150 Å per 4 pixel spectral resolution element.

Table 2. Equivalent Widths (mÅ)^a

Ion	$\lambda(\text{\AA})$	χ (eV)	$\log(gf)$	IV-81	IV-59	IV-82	1-109	1-36	1-31	1-40	G18481 _0316	1-110	G18484 _0309
O I	6300.304	0.000	-9.780	60.0 ^b	70.0 ^b	45.0 ^b	...	20.0 ^b	16.0 ^b	14.0 ^b	16.0 ^b
O I	6363.776	0.020	-10.300	29.0 ^b	19.0 ^b	14.0 ^b
O I	7771.944	9.150	0.369	14.0 ^b	11.0 ^b	17.5 ^b	25.0 ^b	22.0 ^b	27.0 ^b	...	25.0 ^b
O I	7774.166	9.150	0.223	12.0 ^b	9.0 ^b	26.5 ^b	29.0 ^b	19.0 ^b	24.0 ^b	21.5 ^b	18.0 ^b
O I	7775.388	9.150	0.001	10.0 ^b	6.0 ^b	12.0 ^b	10.0 ^b	15.0 ^b
Na I	5682.633	2.100	-0.700	102.5 ^b	71.8 ^b	49.7 ^b	57.1 ^b	45.4 ^b	31.8 ^b	50.4 ^b	16.9 ^b	42.4 ^b	19.3 ^b
Na I	5688.193	2.100	-0.420	121.5 ^b	101.3 ^b	69.2 ^b	78.6 ^b	65.4 ^b	45.9 ^b	70.0 ^b	42.2 ^b	66.4 ^b	31.8 ^b
Na I	5889.950	0.000	0.110	700.0 ^b	470.8 ^b	322.3 ^b	347.0 ^b	309.0 ^b	269.1 ^b	327.2 ^b	257.2 ^b	306.2 ^b	232.5 ^b
Na I	5895.924	0.000	-0.190	539.0 ^b	382.5 ^b	276.3 ^b	285.4 ^b	258.4 ^b	227.1 ^b	271.1 ^b	217.4 ^b	270.7 ^b	202.4 ^b
Na I	6154.225	2.100	-1.530	36.4 ^b	22.3 ^b	6.0 ^b	19.4 ^b	9.0 ^b	6.0 ^b	7.6 ^b
Na I	6160.747	2.100	-1.230	58.7 ^b	35.5 ^b	14.2 ^b	29.6 ^b	17.4 ^b	8.5 ^b	19.9 ^b	6.5 ^b	23.4 ^b	...
Mg I	5528.405	4.340	-0.480	183.8	188.3	157.6	...	131.6	139.7	145.3	128.6	...	109.1
Si I	5421.178	5.620	-1.430	15.8	11.1
Si I	5665.554	4.920	-2.040	24.8	...	19.6	...	15.6	13.5	...	13.1
Si I	5690.427	4.930	-1.870	28.6	28.6	25.4	28.7	21.6	24.3	21.3	18.0
Si I	5701.105	4.930	-2.050	20.8	...	15.3	15.6	...	12.6	...	16.7
Si I	5772.145	5.080	-1.750	21.2	28.4	27.1	22.9	19.5	18.9	18.7	15.0	...	16.7
Si I	5793.071	4.930	-2.060	23.8	24.9	20.8	...	17.1	...	15.6
Si I	5948.540	5.080	-1.230	54.0	61.6	60.5	55.3	48.7	43.4	43.7	36.7	...	23.4
Si I	6145.015	5.610	-1.440	12.8	...	15.0	...	13.8	...	10.3	8.6

^aTable available electronically.

^bLine identified by hand. All other lines are identified automatically.

^cFe I line used in the $\lambda D - W_\lambda$ fit.

Table 3. Solar Abundance Ratios [X/Fe]

Ion	# lines	[X/Fe] ^a (dex)	σ^a (dex)	Δ [us-photospheric] ^b (dex)
O I	2	+1.60	0.08	+0.27
Na I	4	-1.21	0.04	-0.04
Mg I	9	+0.02	0.18	-0.06
Si I	26	+0.09	0.11	+0.04
Ca I	19	-1.30	0.18	-0.16
Sc II	7	-4.24	0.12	+0.09
Ti I	42	-2.52	0.13	-0.04
V I	13	-3.48	0.16	+0.02
Cr I	13	-1.78	0.12	+0.05
Mn I	5	-2.08	0.08	+0.03
Fe I ^c	316	7.44	0.16	-0.06
Fe II ^c	15	7.47	0.08	-0.03
Co I	9	-2.49	0.16	+0.09
Ni I	65	-1.20	0.18	+0.05
Cu I	1	-3.30	...	-0.01
Zn I	1	-2.88	...	+0.02
Zr I	3	-4.61	0.09	+0.29
Ba II	3	-5.31	0.06	+0.06
La II	1	-6.30	...	+0.03 ^d
Eu II	1	-6.92	...	+0.01 ^e

^aMean and 1σ rms deviation about the mean for the abundance in the Sun of the lines of a particular ion using our adopted atomic line parameters.

^bPhotospheric solar abundances from Grevesse & Sauval (1998).

^c $\log \epsilon(\text{Fe})$

^dWe adopt the Solar La abundance of Lawler, Bonvallet & Sneden (2001) ($\epsilon(\text{La}) = +1.14$ dex), which is 0.03 dex smaller than that of Grevesse & Sauval (1998). See the discussion in §4.3.

^eWe adopt the Solar Eu abundance of Lawler *et al.* (2001) ($\epsilon(\text{Eu}) = +0.52$ dex), which is 0.01 dex higher than that of Grevesse & Sauval (1998). See the discussion in §4.3.

Table 4. Stellar Parameters for the M5 Sample.

ID ^a	T_{eff} (K)	$\log(g)$ (dex)	ξ (km/s)
IV-81	4035	0.60	2.06
IV-59	4265	1.00	1.94
IV-82	4375	1.20	1.89
1-109	4635	1.80	1.76
1-36	4755	2.10	1.70
1-31	4880	2.25	1.64
1-40	4810	2.20	1.67
G18484_0316	4995	2.50	1.58
1-110	4875	2.50	1.64
G18484_0309	5325	2.80	1.41
G18450_0453	5170	2.90	1.49
1-32	5066	3.00	1.54
G18458_0547	5090	3.00	1.53
G18447_0453	5275	3.15	1.44
G18155_0228	5270	3.25	1.44
G18564_0457	5400	3.40	1.37
G18445_0448	5300	3.30	1.42
G18483_0608	5300	3.30	1.42
G18279_0101	5335	3.35	1.41
G18569_0455	5825	3.85	1.16
G18152_0232	6000	3.95	1.07
G18487_0606	5930	3.90	1.11
G18172_0750	6100	4.00	1.02
G18279_0107	5785	3.90	1.18
G18175_0749	6000	3.95	1.07

^aIdentifications are from Arp (1962); Buonanno *et al.* (1981) or are assigned based on the J2000 coordinates, rh rm rs.s dd dm dd becoming Grmrss_dmdd.

Table 5a. Iron Abundance and Abundance Ratios: Na – Mg

Star	N _{FeI}	[Fe/H] _I	N _{FeII}	[Fe/H] _{II}	N _O	[O /Fe]	N _{Na}	[Na/Fe]	N _{Mg}	[Mg/Fe]
IV-81	201	-1.28±0.03	9	-1.41±0.05	2	0.37±0.05	6	0.29±0.06	2	0.30±0.12
IV-59	168	-1.32±0.03	9	-1.27±0.05	2	0.25±0.08	6	0.19±0.05	2	0.41±0.05
IV-82	187	-1.35±0.03	9	-1.36±0.05	4	0.28±0.05	6	-0.27±0.05	2	0.23±0.08
1-109	110	-1.35±0.03	3	-1.32±0.05	3	0.09±0.08	6	0.26±0.05	0	...
1-36	160	-1.39±0.03	9	-1.29±0.05	4	0.24±0.13	6	0.15±0.05	2	0.22±0.10
1-31	154	-1.22±0.03	9	-1.25±0.05	4	0.32±0.08	6	-0.20±0.05	2	0.28±0.08
1-40	131	-1.36±0.03	5	-1.33±0.05	4	0.29±0.06	6	0.23±0.05	2	0.34±0.05
G18484_0316	109	-1.30±0.03	6	-1.27±0.05	3	0.36±0.05	5	-0.16±0.05	2	0.26±0.06
1-110	73	-1.38±0.03	4	-1.21±0.05	1	<0.42	5	0.25±0.05	0	...
G18484_0309	83	-1.18±0.03	6	-1.32±0.09	3	0.10±0.05	4	-0.02±0.07	2	0.15±0.10
G18450_0453	80	-1.31±0.03	3	-1.28±0.05	1	<0.64	5	0.30±0.05	1	0.19±0.10
1-32	75	-1.45±0.03	2	-1.30±0.05	1	<0.48	5	0.29±0.06	2	0.22±0.30
G18458_0547	68	-1.44±0.03	5	-1.13±0.12	0	...	5	0.02±0.07	1	0.16±0.10
G18447_0453	52	-1.29±0.05	1	-1.24±0.05	0	...	4	0.18±0.06	2	0.17±0.06
G18144_0228	47	-1.23±0.04	1	-1.27±0.05	0	...	3	-0.26±0.05	2	0.32±0.06
G18564_0457	59	-1.01±0.03	0	...	1	<0.39	4	-0.27±0.07	1	0.19±0.10
G18445_0448	60	-1.27±0.03	4	-1.09±0.05	1	<0.46	4	0.27±0.05	1	0.42±0.10
G18483_0608	51	-1.24±0.03	0	...	1	<0.48	4	0.21±0.05	2	0.38±0.07
G18279_0101	48	-1.18±0.07	1	-1.34±0.05	0	...	4	0.15±0.05	0	...
G18579_0455	10	-1.17±0.08	0	...	0	...	3	0.17±0.10	0	...
G18152_0232	6	-1.13±0.14	0	...	0	...	2	-0.25±0.05	0	...
G18487_0606	6	-1.43±0.08	0	...	0	...	2	0.74±0.18	1	0.39±0.10
G18172_0750	3	-1.00±0.11	0	...	0	...	2	-0.26±0.12	0	...
G18279_0107	7	-1.48±0.12	0	...	0	...	2	0.33±0.12	0	...
G18175_0749	5	-1.22±0.10	0	...	0	...	2	0.40±0.25	0	...
<MS>	0	...	0	...	3	0.22±0.07	0	...	1	0.11±0.10

Table 5b. Abundance Ratios: Si – V

Star	N _{Si}	[Si/Fe]	N _{Ca}	[Ca/Fe]	N _{Sc}	[Sc/Fe]	N _{Ti}	[Ti/Fe]	N _V	[V /Fe]
IV-81	16	0.31±0.06	19	0.28±0.06	7	0.15±0.08	35	0.35±0.04	9	0.01±0.05
IV-59	12	0.24±0.07	17	0.25±0.07	7	0.18±0.06	28	0.08±0.03	9	-0.25±0.06
IV-82	15	0.30±0.05	17	0.33±0.07	7	0.09±0.07	27	0.17±0.03	10	-0.08±0.05
1-109	9	0.27±0.06	15	0.26±0.05	5	0.13±0.06	10	0.09±0.05	4	-0.27±0.06
1-36	16	0.23±0.05	17	0.35±0.05	7	0.15±0.05	14	0.15±0.03	4	-0.14±0.05
1-31	14	0.20±0.06	18	0.32±0.05	7	0.01±0.05	17	0.12±0.03	7	-0.16±0.05
1-40	12	0.25±0.06	18	0.37±0.06	7	0.07±0.07	14	0.14±0.03	3	-0.17±0.05
G18484_0316	14	0.19±0.05	18	0.40±0.06	7	0.03±0.05	9	0.14±0.05	2	-0.01±0.10
1-110	5	0.15±0.06	16	0.31±0.05	6	0.22±0.09	4	0.12±0.05	1	-0.40±0.10
G18484_0309	9	0.28±0.11	18	0.31±0.05	5	-0.15±0.07	5	0.21±0.05	0	...
G18450_0453	6	0.19±0.07	17	0.40±0.07	5	-0.04±0.07	6	0.24±0.05	0	...
1-32	4	0.12±0.08	18	0.40±0.05	5	0.15±0.05	4	0.20±0.05	1	0.01±0.10
G18458_0547	3	0.15±0.12	15	0.42±0.06	4	0.11±0.05	2	0.13±0.07	1	-0.15±0.10
G18447_0453	3	0.19±0.11	11	0.41±0.07	2	-0.28±0.13	1	0.34±0.10	0	...
G18144_0228	6	0.22±0.10	12	0.28±0.06	3	-0.08±0.05	1	0.31±0.10	0	...
G18564_0457	5	99.00±0.00	15	0.26±0.06	1	-0.12±0.10	4	0.15±0.11	0	...
G18445_0448	6	0.17±0.08	18	0.43±0.05	4	0.02±0.05	2	0.24±0.13	0	...
G18483_0608	3	99.00±0.00	14	0.33±0.05	2	-0.03±0.05	4	0.14±0.09	0	...
G18279_0101	2	0.06±0.07	12	0.24±0.09	2	0.03±0.20	3	-0.06±0.11	0	...
G18579_0455	0	...	2	0.29±0.22	0	...	0	...	0	...
G18152_0232	0	...	2	-0.17±0.23	0	...	0	...	0	...
G18487_0606	0	...	2	0.39±0.30	0	...	0	...	0	...
G18172_0750	0	...	3	-0.05±0.17	0	...	0	...	0	...
G18279_0107	0	...	3	0.12±0.16	0	...	0	...	0	...
G18175_0749	0	...	2	0.17±0.15	0	...	0	...	0	...
<MS>	0	...	0	...	2	-0.27±0.08	0	...	0	...

Table 5c. Abundance Ratios: Cr – Cu

Star	N _{Cr}	[Cr/Fe]	N _{Mn}	[Mn/Fe]	N _{Co}	[Co/Fe]	N _{Ni}	[Ni/Fe]	N _{Cu}	[Cu/Fe]
IV-81	9	0.02±0.07	3	-0.16±0.10	6	0.06±0.10	46	-0.08±0.04	1	-0.45±0.10
IV-59	4	-0.24±0.15	3	-0.49±0.06	5	-0.10±0.10	36	-0.02±0.05	1	-0.51±0.10
IV-82	7	0.04±0.09	3	-0.40±0.07	5	-0.08±0.08	40	-0.10±0.04	1	-0.50±0.10
1-109	1	-0.32±0.10	0	...	2	0.03±0.20	24	-0.21±0.05	0	...
1-36	3	-0.01±0.20	3	-0.32±0.07	2	0.03±0.11	32	-0.17±0.05	1	-0.54±0.10
1-31	4	-0.16±0.07	2	-0.44±0.06	1	-0.11±0.10	34	-0.18±0.04	1	-0.56±0.10
1-40	4	-0.05±0.10	2	-0.48±0.06	2	0.07±0.15	25	-0.16±0.05	1	-0.57±0.10
G18484_0316	4	-0.02±0.05	2	-0.32±0.05	1	0.05±0.10	25	-0.08±0.05	1	-0.63±0.10
1-110	0	...	0	...	1	-0.17±0.10	16	-0.17±0.07	0	...
G18484_0309	1	-0.19±0.10	0	...	1	-0.26±0.10	17	-0.17±0.07	0	...
G18450_0453	1	-0.02±0.10	2	-0.38±0.10	0	...	15	-0.13±0.07	0	...
1-32	1	-0.35±0.10	1	-0.41±0.10	0	...	13	-0.07±0.06	0	...
G18458_0547	1	-0.41±0.10	0	...	0	...	12	-0.02±0.10	0	...
G18447_0453	1	-0.50±0.10	0	...	0	...	6	-0.02±0.19	0	...
G18144_0228	0	...	0	...	0	...	5	-0.22±0.15	0	...
G18564_0457	0	...	0	...	0	...	7	-0.27±0.15	0	...
G18445_0448	1	-0.03±0.10	0	...	0	...	9	-0.04±0.13	0	...
G18483_0608	0	...	0	...	0	...	6	-0.25±0.15	0	...
G18279_0101	0	...	0	...	0	...	4	-0.43±0.27	0	...
G18579_0455	0	...	0	...	0	...	0	...	0	...
G18152_0232	0	...	0	...	0	...	0	...	0	...
G18487_0606	0	...	0	...	0	...	0	...	0	...
G18172_0750	0	...	0	...	0	...	0	...	0	...
G18279_0107	0	...	0	...	0	...	0	...	0	...
G18175_0749	0	...	0	...	0	...	0	...	0	...
<MS>	0	...	0	...	0	...	0	...	0	...

Table 5d. Abundance Ratios: Zn – Eu

Star	N _{Zn}	[Zn/Fe]	N _{Zr}	[Zr/Fe]	N _{Ba}	[Ba/Fe]	N _{La}	[La/Fe]	N _{Eu}	[Eu/Fe]
IV-81	0	...	3	0.19±0.05	3	0.03±0.05	2	0.23±0.06	1	0.61±0.10
IV-59	1	0.43±0.10	2	-0.23±0.05	3	0.22±0.09	0	...	1	0.54±0.10
IV-82	0	...	2	-0.25±0.05	3	-0.01±0.05	1	0.22±0.10	1	0.55±0.10
1-109	0	...	0	...	3	-0.13±0.07	0	...	0	...
1-36	0	...	0	...	3	0.01±0.05	1	-0.01±0.10	1	0.60±0.10
1-31	0	...	0	...	3	-0.11±0.05	0	...	1	0.53±0.10
1-40	0	...	0	...	3	-0.03±0.05	0	...	0	...
G18484_0316	0	...	0	...	3	-0.14±0.05	0	...	0	...
1-110	0	...	0	...	3	-0.09±0.07	0	...	0	...
G18484_0309	0	...	0	...	3	-0.11±0.05	0	...	1	0.52±0.10
G18450_0453	0	...	0	...	3	0.04±0.05	0	...	0	...
1-32	0	...	0	...	3	0.02±0.05	0	...	0	...
G18458_0547	0	...	0	...	3	0.04±0.05	0	...	0	...
G18447_0453	0	...	0	...	3	-0.09±0.09	0	...	0	...
G18144_0228	0	...	0	...	3	-0.12±0.13	0	...	0	...
G18564_0457	0	...	0	...	3	-0.27±0.05	0	...	0	...
G18445_0448	0	...	0	...	3	-0.05±0.05	0	...	0	...
G18483_0608	0	...	0	...	3	-0.17±0.05	0	...	0	...
G18279_0101	0	...	0	...	3	-0.22±0.10	0	...	0	...
G18579_0455	0	...	0	...	2	-0.31±0.10	0	...	0	...
G18152_0232	0	...	0	...	3	-0.47±0.17	0	...	0	...
G18487_0606	0	...	0	...	2	-0.22±0.17	0	...	0	...
G18172_0750	0	...	0	...	1	-0.65±0.11	0	...	0	...
G18279_0107	0	...	0	...	2	0.02±0.15	0	...	0	...
G18175_0749	0	...	0	...	0	...	0	...	0	...
<MS>	0	...	0	...	0	...	0	...	0	...

Table 6. Sensitivity of Abundance

	ΔW_λ 10%	ΔT_{eff} + 100 K	$\Delta \log(g)$ + 0.2 dex	$\Delta \xi$ + 0.3 km s ⁻¹	$\Delta [\text{Fe}/\text{H}]$ + 0.2 dex
Fe I :					
4250/1.5/1.8	0.10	0.06	0.02	-0.09	-0.01
5000/3.0/1.5	0.10	0.09	0.00	-0.07	0.00
6000/4.0/1.0	0.11	0.08	-0.02	-0.06	0.00
Fe II:					
4250/1.5/1.8	0.06	-0.11	0.10	-0.03	-0.06
5000/3.0/1.5	0.06	-0.04	0.09	-0.03	-0.05
O I(permitted):					
4250/1.5/1.8	0.08	-0.20	0.10	-0.02	-0.01
5000/3.0/1.5	0.07	-0.12	0.07	-0.02	-0.01
O I(forbidden):					
4250/1.5/1.8	0.05	0.02	0.08	0.00	-0.07
5000/3.0/1.5	0.05	0.03	0.07	0.00	-0.06
Na I :					
4250/1.5/1.8	0.14	0.14	-0.03	-0.05	0.00
5000/3.0/1.5	0.09	0.11	-0.05	-0.02	-0.01
6000/4.0/1.0	0.09	0.08	-0.05	0.00	0.00
Mg I :					
4250/1.5/1.8	0.19	0.06	0.00	-0.13	0.01
5000/3.0/1.5	0.12	0.08	-0.02	-0.06	0.00
Si I :					
4250/1.5/1.8	0.07	-0.04	0.04	-0.03	-0.03
5000/3.0/1.5	0.06	0.01	0.01	-0.01	-0.01
Ca I :					
4250/1.5/1.8	0.16	0.13	-0.02	-0.13	0.02
5000/3.0/1.5	0.11	0.09	-0.03	-0.06	0.01
6000/4.0/1.0	0.11	0.08	-0.06	-0.06	0.00
Sc II:					
4250/1.5/1.8	0.11	-0.02	0.08	-0.07	-0.06
5000/3.0/1.5	0.07	0.00	0.08	-0.03	-0.05
Ti I :					
4250/1.5/1.8	0.07	0.17	0.00	-0.03	0.01

Table 6—Continued

	ΔW_λ 10%	ΔT_{eff} + 100 K	$\Delta \log(g)$ + 0.2 dex	$\Delta \xi$ + 0.3 km s ⁻¹	$\Delta[\text{Fe}/\text{H}]$ + 0.2 dex
5000/3.0/1.5	0.06	0.12	0.00	-0.01	0.01
V I :					
4250/1.5/1.8	0.07	0.20	0.00	-0.03	0.01
5000/3.0/1.5	0.04	0.15	0.00	0.00	0.01
Cr I :					
4250/1.5/1.8	0.08	0.11	0.00	-0.01	0.01
5000/3.0/1.5	0.16	0.15	-0.02	-0.13	0.02
Mn I :					
4250/1.5/1.8	0.08	0.14	0.00	-0.01	0.00
5000/3.0/1.5	0.05	0.09	0.00	0.00	0.00
Co I :					
4250/1.5/1.8	0.06	0.08	0.03	-0.01	-0.02
5000/3.0/1.5	0.06	0.11	0.01	0.00	0.00
Ni I :					
4250/1.5/1.8	0.09	0.03	0.03	-0.06	-0.03
5000/3.0/1.5	0.07	0.08	0.01	-0.03	0.00
Cu I :					
4250/1.5/1.8	0.07	0.08	0.03	-0.01	-0.02
5000/3.0/1.5	0.05	0.10	0.01	0.00	0.00
Zn I :					
4250/1.5/1.8	0.05	-0.08	0.06	-0.01	-0.03
Zr I :					
4250/1.5/1.8	0.04	0.22	0.00	-0.01	0.01
Ba II:					
4250/1.5/1.8	0.23	0.02	0.07	-0.25	-0.06
5000/3.0/1.5	0.15	0.02	0.07	-0.16	-0.06
6000/4.0/1.0	0.12	0.05	0.05	-0.13	-0.01
La II:					
4250/1.5/1.8	0.06	0.01	0.08	-0.02	-0.07
Eu II:					
4250/1.5/1.8	0.06	-0.02	0.09	-0.02	-0.07
5000/3.0/1.5	0.05	0.00	0.08	-0.02	-0.06

Table 7. Mean Iron Abundance and Abundance Ratios.

	# stars	$\langle[X/Fe]\rangle$ (dex)	σ_{obs} (dex)	σ_{pred} (dex)
Fe I ^a	25	-1.30 ± 0.02	0.12	0.14
Fe II ^a	17	-1.28 ± 0.02	0.08	0.14
O I	9	$+0.26\pm0.03$	0.10	0.05
Na I	25	$+0.08\pm0.05$	0.26	0.12
Mg I	13	$+0.29\pm0.02$	0.09	0.12
Si I	17	$+0.21\pm0.02$	0.07	0.07
Ca I	25	$+0.33\pm0.03$	0.14	0.08
Sc II	19	$+0.05\pm0.03$	0.13	0.14
Ti I	19	$+0.16\pm0.02$	0.10	0.11
V I	11	-0.14 ± 0.04	0.12	0.13
Cr I	14	-0.13 ± 0.05	0.17	0.15
Mn I	9	-0.39 ± 0.03	0.10	0.11
Co I	10	-0.06 ± 0.03	0.11	0.09
Ni I	19	-0.12 ± 0.02	0.10	0.05
Cu I	7	-0.53 ± 0.02	0.05	0.10
Zn I	1	+0.43	...	0.08
Zr I	3	-0.10 ± 0.12	0.20	0.19
Ba II	24	-0.08 ± 0.04	0.13	0.18
La II	3	$+0.18\pm0.07$	0.11	0.14
Eu II	6	$+0.56\pm0.02$	0.04	0.16

^aFor Fe, [Fe/H] is given. For all other elements, [X/Fe] is given.

Table 8. Comparison of Our Abundance Analysis For M5 With Earlier Work

[X/Fe]	Snedden <i>et al.</i> (1992) (dex)	Ivans <i>et al.</i> (2001) (dex)	This work (dex)	σ_c (dex)
Fe I ^a	-1.17 ± 0.01	-1.34 ± 0.01	-1.30 ± 0.02	0.11
Fe II ^a	-1.16 ± 0.02	-1.21 ± 0.01	-1.28 ± 0.02	0.14
O I	$+0.11 \pm 0.06$	$+0.02 \pm 0.04$	$+0.26 \pm 0.03$	0.03
Na I	-0.07 ± 0.06	$+0.11 \pm 0.03$	$+0.08 \pm 0.05$	0.08
Mg I	...	$+0.34 \pm 0.03$	$+0.29 \pm 0.02$	0.04
Si I	$+0.20 \pm 0.02$	$+0.31 \pm 0.01$	$+0.21 \pm 0.02$	0.06
Ca I	$+0.19 \pm 0.01$	$+0.26 \pm 0.01$	$+0.33 \pm 0.03$	0.05
Sc II	-0.10 ± 0.03	-0.01 ± 0.02	$+0.05 \pm 0.03$	0.13
Ti I	$+0.29 \pm 0.04$	$+0.22 \pm 0.02$	$+0.16 \pm 0.02$	0.10
V I	$+0.05 \pm 0.03$	-0.10 ± 0.02	-0.14 ± 0.04	0.12
Mn I	...	-0.25 ± 0.02	-0.39 ± 0.03	0.09
Ni I	-0.10 ± 0.02	-0.05 ± 0.01	-0.12 ± 0.02	0.05
Ba II	...	$+0.16 \pm 0.02$	-0.08 ± 0.04	0.15
La II	...	$+0.02 \pm 0.02$	$+0.18 \pm 0.07$	0.12
Eu II	...	$+0.43 \pm 0.02$	$+0.56 \pm 0.02$	0.15

^aFor Fe, [Fe/H] is given. For all other elements, [X/Fe] is given.

Table 9. Updated Mean Iron Abundance and Abundance Ratios in M71.

	# stars	$\langle [X/Fe] \rangle$ (dex)	σ_{obs} (dex)	σ_{pred} (dex)
Fe I ^a	25	-0.63 ± 0.02	0.08	0.16
Fe II ^a	25	-0.73 ± 0.03	0.13	0.21
C I	6	$+1.36 \pm 0.20$	0.49	0.13
O I	25	$+0.10 \pm 0.04$	0.18	0.12
Na I	25	$+0.10 \pm 0.03$	0.14	0.10
Mg I	24	$+0.35 \pm 0.02$	0.10	0.12
Al I	11	$+0.22 \pm 0.03$	0.10	0.10
Si I	24	$+0.27 \pm 0.03$	0.14	0.17
K I	11	-0.12 ± 0.09	0.30	0.29
Ca I	25	$+0.36 \pm 0.02$	0.09	0.11
Sc II	25	$+0.03 \pm 0.03$	0.16	0.15
Ti I	25	$+0.23 \pm 0.02$	0.12	0.11
V I	21	$+0.04 \pm 0.02$	0.14	0.17
Cr I	23	-0.07 ± 0.02	0.09	0.09
Mn I	13	-0.28 ± 0.03	0.11	0.11
Co I	17	-0.07 ± 0.01	0.05	0.10
Ni I	25	$+0.01 \pm 0.01$	0.06	0.09
Cu I	21	-0.07 ± 0.03	0.14	0.21
Zn I	8	$+0.40 \pm 0.06$	0.16	0.22
Y II	3	-0.07 ± 0.02	0.04	0.15
Zr I	10	-0.04 ± 0.08	0.25	0.16
Ba II	25	$+0.19 \pm 0.02$	0.12	0.19
La II	14	$+0.13 \pm 0.03$	0.10	0.15
Eu II	11	$+0.36 \pm 0.05$	0.31	0.11

^aFor Fe, $[Fe/H]$ is given. For all other elements, $[X/Fe]$ is given.